JEM Journal of Experimental Medicine

ARTICLE

Syk degradation restrains plasma cell formation and promotes zonal transitions in germinal centers

Natalia Davidzohn[1], Adi Biram[1], Liat Stoler-Barak[1], Amalie Grenov[1], Bareket Dassa[2], and Ziv Shulman[1]

Germinal centers (GCs) are sites at which B cells proliferate and mutate their antibody-encoding genes in the dark zone (DZ), followed by affinity-based selection in the light zone (LZ). B cell antigen receptor (BCR) signals induce Syk activation followed by rapid phosphatase-mediated desensitization; however, how degradation events regulate BCR functions in GCs is unclear. Here, we found that Syk degradation restrains plasma cell (PC) formation in GCs and promotes B cell LZ to DZ transition. Using a mouse model defective in Cbl-mediated Syk degradation, we demonstrate that this machinery attenuates BCR signaling intensity by mitigating the Kras/Erk and PI3K/Foxo1 pathways, and restricting the expression of PC transcription factors in GC B cells. Inhibition of Syk degradation perturbed gene expression, specifically in the LZ, and enhanced the generation of PCs without affecting B cell proliferation. These findings reveal how long-lasting attenuation of signal transduction by degradation events regulates cell fate within specialized microanatomical sites.

Introduction

Effective enduring protection from invading pathogens depends on formation of long-lived plasma cells (PCs) that secrete high-affinity antibodies, and memory B cells that rapidly differentiate into antibody-forming cells upon secondary exposure (Victora and Nussenzweig, 2012; Weisel and Shlomchik, 2017). These cells are generated in microanatomical sites known as germinal centers (GCs) that form within secondary lymphoid organs in response to invading microbes or vaccination (Berek et al., 1991; MacLennan, 1994). GCs are divided into two distinct functional zones, a dark zone (DZ) in which B cells proliferate and introduce mutations into their immunoglobulin genes, and a light zone (LZ), where B cells encounter antigen on the surface of follicular dendritic cells (FDCs), and are subjected to affinity-based selection (MacLennan, 1994; Allen et al., 2007a; Victora and Nussenzweig, 2012). Following cell division in the DZ, B cells migrate to the LZ, where their newly mutated B cell receptors (BCRs) interact with and capture antigen for processing and presentation to cognate T cells as peptides on surface MHCII molecules. These specialized T cells, known as T follicular helper cells, physically interact with cognate B cells and deliver help signals in the form of secreted cytokines and surface-bound molecules (Victora and Nussenzweig, 2012). Furthermore, several studies demonstrated that in addition to antigen uptake (Batista and Neuberger, 2000; Kwak et al., 2018), BCR affinity and triggering of downstream signals play important roles in the GC functions (Phan et al., 2003; Kräutler et al., 2017; Suan et al., 2017; Luo et al., 2018, 2019; Ise and Kurosaki, 2019; Shlomchik et al., 2019); however, how modulation of signal transduction intensities regulates B cell fate within specific GC zones and promotes generation of PCs is incompletely understood.

Previous studies demonstrated that BCR signaling in GC B cells is rewired and is significantly less efficient in triggering phosphorylation events of most downstream factors than in their naive counterparts (Khalil et al., 2012). B cells that receive T cell help up-regulate the transcription factor Myc, which is required for reentry of LZ B cells into the DZ and for subsequent clonal expansion (Dominguez-Sola et al., 2012; Calado et al., 2012; De Silva and Klein, 2015). Combination of BCR and CD40 signals leads to maximal expression of Myc in GC B cells, indicating that B cell selection in GCs depends on synergistic signals from T cells and the BCR for enhanced proliferation in the DZ (Luo et al., 2018). Expression of Foxo1 is critical for acquisition of the DZ phenotype, and in its absence, antibody affinity maturation is perturbed (Sander et al., 2015; Dominguez-Sola et al., 2015). BCR triggering induces inactivation of Foxo1 by phosphorylation (Yusuf et al., 2004; Herzog et al., 2009; Srinivasan et al., 2009), and therefore, it is expected that antigen engagements in the LZ would restrain transition to the DZ. Together, these findings suggest that an additional unknown mechanism is involved in BCR signal transduction that allows both Foxo1 inactivation and interzonal migration.

[1]Department of Immunology, Weizmann Institute of Science, Rehovot, Israel; [2]Department of Life Science Core Facilities, Weizmann Institute of Science, Rehovot, Israel.

Correspondence to Ziv Shulman: ziv.shulman@weizmann.ac.il.

The BCR complex includes the two amplifying adaptors, Igα and Igβ, that contain immuno-tyrosine activating motifs (ITAMs) in their cytoplasmic domains (Reth and Wienands, 1997; Dal Porto et al., 2004). Receptor ligation induces rapid phosphorylation of these sites and recruitment of the key kinase, spleen tyrosine kinase (Syk), which binds the phosphorylated ITAMs via its SH2 domains (Mócsai et al., 2010; Satpathy et al., 2015). These events lead to rapid Syk autophosphorylation at multiple tyrosines, most of which were shown to play an important role in BCR signal transduction (Reth and Wienands, 1997; Kulathu et al., 2009; Song et al., 2016). Subsequent rapid down-regulation of the immunoglobulin signals depends on its inactivation by several distinct mechanisms (Pao et al., 1997; Kulathu et al., 2009; Mócsai et al., 2010; Luo et al., 2019). Phosphatases dephosphorylate Syk and its downstream targets, and attenuate the BCR signaling pathway in both naive and GC B cells (Dustin et al., 1999; Adachi et al., 2001; Khalil et al., 2012). Furthermore, Akt phosphorylation activates a negative feedback loop that attenuates the magnitude of BCR signaling (Luo et al., 2019). An additional and less explored mechanism that restricts BCR signaling is through degradation of key signaling molecules. Phosphorylation of Syk at tyrosine 317 leads to recruitment of the E3 ubiquitin ligase Casitas B-lineage lymphoma (Cbl), which tags Syk for degradation through its ubiquitylation (Lupher et al., 1998; Rao et al., 2002; Sohn et al., 2003). However, how this mechanism regulates B cell fate within the GC, including interzonal transitions and generation of PCs, remains unknown.

Here, we found that BCR triggering and extended signaling through Syk promote PC generation and impede B cell LZ to DZ transition, whereas rapid Syk degradation in the LZ attenuates signal transduction intensity and promotes B cell progression to a DZ cell state. Inhibition of Syk degradation enhanced the activation of the Kras and PI3K pathways and modulated gene expression specifically in the LZ. Collectively, our findings describe a mechanism of signal transduction attenuation in GCs that is different from the previously described kinase- and phosphatase-mediated desensitization processes.

Results

A mouse model for analysis of Cbl-mediated Syk degradation

BCR engagement by cognate antigen triggers a series of phosphorylation events with many targets, including Syk, that amplify the receptor signals and propagate downstream signaling cascades (Mócsai et al., 2010). Syk phosphorylation at tyrosine 317 (Y317) is essential for its interaction with the E3 ligase Cbl (Yankee et al., 1999) followed by rapid Syk ubiquitylation and degradation (Geahlen, 2009; Lupher et al., 1998; Sohn et al., 2003; Fig. 1 A). To explore the physiological role of this molecular mechanism in BCR signaling and GC dynamics, we generated a new mouse strain using CRISPR/Cas9 mutagenesis to introduce a point mutation into the *SYK* gene to abolish Cbl interaction with phosphorylated Syk protein (Syk^{Y317F}; Fig. 1 B; Mócsai et al., 2010). The advantage of this new model over conditional activation of the BCR pathway in transgenic mice is that it allowed us to examine the role of Syk functions specifically upon Syk activation, whereas nonphosphorylated Syk is expected to be unaffected by this perturbation. To verify whether Syk degradation is indeed interrupted in our new model, freshly isolated follicular B cells derived from Syk^{Y317F} and WT mice were stimulated by anti-IgM for 2 and 5 min, and total Syk protein levels were examined by Western blot analysis. Consistent with previous findings that show Syk ubiquitylation 2 min after BCR triggering and Cbl-mediated degradation in cell lines (Lupher et al., 1998; Sohn et al., 2003; Geahlen, 2009; Satpathy et al., 2015), Syk levels declined in WT B cells by ∼50% after 2 and 5 min of immunoglobulin stimulation, whereas almost no reduction in Syk levels was observed in Syk^{Y317F} B cells (Fig. 1, C and D).

To assess how inhibition of Syk degradation affects the magnitude of BCR signaling, we examined the changes in intracellular calcium levels in response to BCR triggering by loading the cells with the ratiometric calcium indicator, Indo-1, followed by stimulation with a high or low dose of anti-IgM antibody. While WT B cells showed a typical transient increase followed by a decrease in intracellular calcium levels in response to stimulation at either dose, Syk^{Y317F} B cells showed elevated intracellular calcium levels for up to 10 min after BCR triggering (Fig. 1 E). To examine how prolonged BCR signaling through inhibition of Syk degradation affects B cell activation, we stimulated B cells with anti-IgM for 16 h and examined the expression of the typical activation marker, CD86, by flow cytometry. We found that in stimulated Syk^{Y317F} B cells, CD86 expression was twofold higher compared with WT B cells (Fig. 1 F). Thus, Syk degradation restrains the duration of BCR signaling period and attenuates B cell activation.

Ligation of the BCR triggers downstream signaling followed by internalization of the receptor. High levels of immunoglobulin expression on the surface of the B cells, as well as defects in BCR internalization can lead to enhanced immune-receptor signaling (Gazumyan et al., 2006). To rule out this possibility, we stimulated cells with biotinylated anti-IgM antibody, and tracked cell surface BCR by staining the stimulating antibody with fluorescent streptavidin. Flow cytometry analysis of nonstimulated B cells revealed that Syk^{Y317F} B cells expressed ∼30% less IgM receptor compared with WT B cells (Fig. S1). However, in response to anti-IgM stimulation, we did not detect defects in global BCR internalization over time (Fig. 1 G). Furthermore, we found that the BCR-induced Syk autophosphorylation of tyrosine 348, which forms a binding site for downstream effectors (Kulathu et al., 2009; Mócsai et al., 2010), was unaffected by deletion of the tyrosine at position 317 (Fig. S1). Collectively, we conclude that prolonged BCR signaling in Syk^{Y317F} B cells was a result of the disruption in Syk degradation rather than enhanced immunoglobulin expression or defects in its internalization.

Syk^{Y317F} mice contain abnormally high levels of PCs and serum immunoglobulins

BCR signaling regulates B cell development in the bone marrow (BM), and a defect in downstream signals, including those of Syk, leads to severe deficiency in the generation of mature B cells (Turner et al., 1995; Cheng et al., 1995). Furthermore, it was demonstrated that Cbl-deficient mice show altered B cell development; however, it remains unclear which Cbl targets are

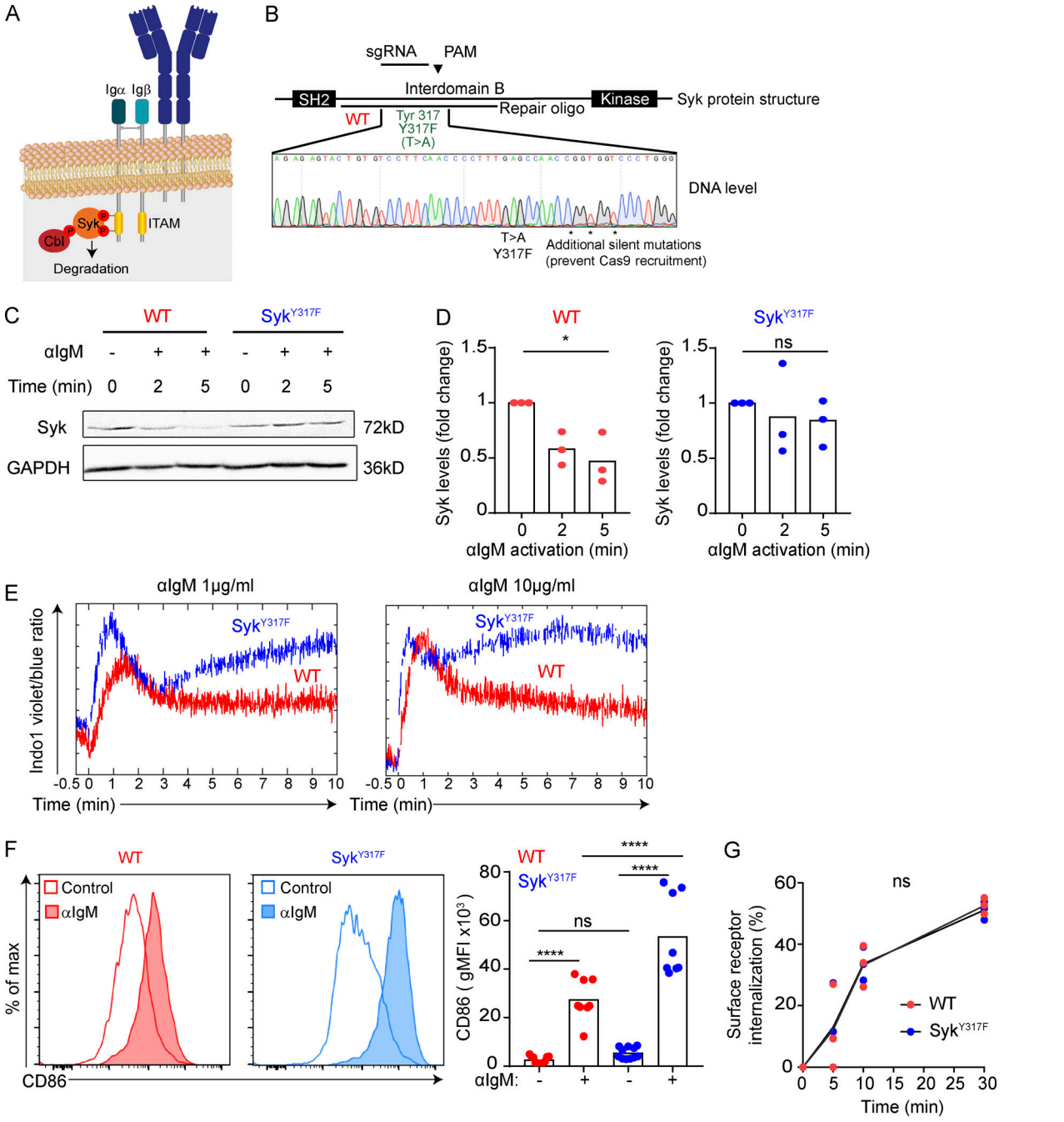

Figure 1. **Syk degradation attenuates B cell antigen receptor signaling and B cell activation. (A)** A scheme of the BCR complex and its interactions with Syk and Cbl. **(B)** Gene targeting strategy for generating mice carrying a point mutation (Y317F) in Syk. **(C and D)** Freshly purified follicular B cells derived from WT and Syk^{Y317F} mice were stimulated with anti-IgM for 0, 2, or 5 min, and Syk protein levels were examined. **(C)** A representative blot is shown of three independent experiments. **(D)** Quantification with signals normalized to GAPDH and to unstimulated cells. Bars depict means. *n* = 3, three independent experiments, one-way ANOVA. **(E)** Analysis of intracellular Ca^{2+} in Syk^{Y317F} and WT B cells that were loaded with Indo-1 and stimulated with 1 or 10 µg/ml αIgM. A representative result of two independent experiments is shown. **(F)** Flow cytometry histograms and quantification of CD86 expression in WT and Syk^{Y317F} B cells with or without αIgM stimulation (10 µg/ml). Each dot in the graphs represents a single repetition; bars represent the mean (*n* = 8, two independent experiments, one-way ANOVA). **(G)** B cells were stimulated with biotin-conjugated αIgM and the levels of surface immunoglobulin were examined by staining with streptavidin–Alexa Fluor 647 at different time points (*n* = 3, one experiment, two-way ANOVA). *, P = 0.05; ****, P < 0.0001; ns, not significant. ITAM, immuno-tyrosine activating motif; PAM, protospacer adajacent motif; max, maximum.

involved in this process, and whether Syk plays a role (Kitaura et al., 2007). To address the role of Syk degradation under physiological conditions, we first examined the different B cell developmental stages in WT and Syk^{Y317F} mice within different organs. Flow-cytometric analysis of B cells derived from the BM compartment of these mice revealed no defect in formation of pre- and pro-B cells (B220$^+$IgM$^-$) or in the generation of immature and mature B cells (IgM$^+$IgD$^-$ and IgM$^+$IgD$^+$,

respectively; Fig. S2 A). The different developmental stages of B cells in the circulation were intact as well (Fig. S2 B). Furthermore, the frequency of T1 ($CD21^{-}CD24^{+}$), T2 ($CD21^{+}CD24^{+}CD23^{+}$), follicular mature ($CD21^{int}CD24^{int}$), and marginal zone ($CD21^{+}CD24^{+}CD23^{-}$) B cell subpopulations in the spleen was largely normal in Syk^{Y317F} mice (Fig. S2 C). Most importantly, the frequencies of mature B cells as well as cells that typically do not express Syk, such as mature CD4 and CD8 T cells in Syk^{Y317F} mice, were similar to those in WT mice (Fig. 2 A). Thus, B cell development in the BM and maturation in the spleen, as well as generation of T lymphocytes, are not defective in Syk^{Y317F} mice.

Enhanced BCR signaling can lead to the development of autoimmune responses, which include generation of spontaneous GCs and antibody-forming cells in response to self-proteins, as well as to an exaggerated response to foreign antigens (Rawlings et al., 2017). Flow-cytometric analysis of unimmunized Syk^{Y317F} mice revealed that spontaneous GCs were slightly smaller in the spleen compared with their WT counterparts, suggesting that these mice do not develop T cell–dependent autoimmunity (Fig. 2 B). Nevertheless, we found an abnormally high frequency of $CD138^{+}$ PCs in the spleen of Syk^{Y317F} mice (Fig. 2 C). Accordingly, analysis of serum immunoglobulins by ELISA revealed that Syk^{Y317F} mice show high titers of IgM and IgA in their serum compared with WT mice (Fig. 2 D). IgG1, an antibody isotype that highly depends on T cell functions for its generation, was also elevated in the Syk^{Y317F} mice (Fig. 2 D). Although B cells are the main cell type expressing Syk, other immune cells express this kinase as well (Mócsai et al., 2010). To examine whether the increase in the presence of PCs in Syk^{Y317F} mice is a result of an intrinsic defect in Syk degradation, specifically in B cells, we generated mixed BM chimeric mice, wherein irradiated WT mice were reconstituted with ∼70% GFP WT and ∼30% Syk^{Y317F} BM-derived cells. In spite of the WT frequency advantage in the follicular compartment, flow-cytometric analysis revealed that most of the PCs in the spleen and BM of the chimeric mice were derived from the Syk^{Y317F} BM cells (Fig. 2 E). Normalization of the PC frequency to the follicular compartment revealed that Syk^{Y317F} PCs were over-represented in both the spleen and the BM compartments (Fig. 2 E). GCs give rise to both plasma and memory cells. Strikingly, as opposed to the increase in PCs and IgG1 serum antibodies, we did not find a similar increase in memory B cells in the BM ($IgG1^{+}$ $CD38^{+}$) of chimeric mice (Fig. 2 F). We conclude that disruption of Syk degradation specifically in B cells results in enhanced PC generation, whereas B cell development and memory cell formation are largely unaffected by this perturbation.

B cell persistence in GCs depends on Syk degradation

Our findings demonstrate that serum IgG1 as well as the pool of BM-resident antibody forming cells, which includes long-lived PCs, are increased in Syk^{Y317F} mice, suggesting that Syk degradation plays a role in T cell–dependent immune responses. To examine this hypothesis, we generated mixed BM chimeric mice (∼50:50 WT and Syk^{Y317F}) and induced a T cell–dependent immune response by subcutaneous immunization with 4-hydroxy-3-nitrophenylacetyl (NP)–KLH in alum into the hind footpads. Flow-cytometric analysis of the GC compartment in popliteal LNs, 7 d later, revealed that the frequency of Syk^{Y317F} and WT B cells was similar to their initial proportions in the follicular compartment (Fig. 3 A). Nonetheless, analysis of the GC compartment after an additional 7 or 14 d revealed that the frequency of Syk^{Y317F} B cells was significantly reduced in the GC reaction (Fig. 3 A). This suggests that Syk degradation is required for B cell persistence and/or retention within the GC.

To further examine the role of Syk degradation in the early stages of the response, we examined the clonal composition of the GC B cells by single-cell immunoglobulin sequencing. We found that the V-region usage was similar between WT and Syk^{Y317F} B cells in the GC (Fig. 3 B). In addition, clonal analysis based on the CDR3 sequence clustering did not reveal abnormal clonal diversity and expansion in Syk^{Y317F} B cells 7 d after the immunization (Fig. 3 C). The proportion of GC Syk^{Y317F} B cells that express IgG1 and the amount of their surface BCR were similar to those observed for WT GC B cells (Fig. S1 B). Staining of GC cells with an antigen (NP-PE) revealed that the proportion of total NP-specific $IgG1^{+}$ B cells was similar between WT and Syk^{Y317F} B cells in the GCs of the chimeric mice (Fig. 3 D). Together, we conclude that Syk degradation did not play a significant role in initial GC seeding; however, retention in the GC reaction was severely impaired in Syk^{Y317F} B cells.

Our findings raise the possibility that affinity maturation might be defective in Syk^{Y317F} B cells. To test this hypothesis, we compared the ability of WT and Syk^{Y317F} GC B cells to acquire somatic hypermutations (SHM) and affinity-enhancing nucleotide changes in the *Igh* of single GC B cells. Immunization of C57BL/6 mice with NP hapten conjugated to a protein carrier triggers an immune response that is dominated by Igλ B cells expressing NP-specific BCR (Cumano and Rajewsky, 1986). Typically, these cells express the *V186.2* V_H gene, and introduction of either of two mutations at specific locations (W33L and K59R) dramatically increases the affinity of their BCR and promotes clonal expansion (Allen et al., 1988; Furukawa et al., 1999). To examine whether Syk^{Y317F} B cells can acquire affinity-enhancing SHM, we immunized WT and Syk^{Y317F} mice with NP-OVA, and sorted single $IgG1^{+}$ $Igλ^{+}$ GC B cells for *Igh* mRNA sequencing. Analysis of the V186.2 mRNA transcripts revealed that Syk^{Y317F} GC B cells accumulate SHM in their *Igh* variable regions to a similar extent as WT GC B cells (Fig. 3 E), and that the frequency of WT and Syk^{Y317F} B cells that acquired one of the affinity-enhancing mutations (W33L or K59R) was similar (Fig. 3 F). We next examined whether the decline in the frequency of Syk^{Y317F} cells in the GCs is a result of ineffective cell division. Immunized chimeric mice were injected with the nucleoside analog 5-ethynyl-2′-deoxyuridine (EdU), which is incorporated into newly formed DNA strands. Flow-cytometric analysis of the GC cells 2.5 or 24 h after EdU injection revealed that WT and Syk^{Y317F} B cells incorporated EdU to a similar extent (Fig. 3 G). Together, we conclude that the dilution of Syk^{Y317F} B cells from the GC cannot be explained by reduced proliferation rate or inability to acquire affinity-enhancing mutations.

To gain more insights about the role of Syk decay in antigen-specific B cells, we examined the role of Syk degradation in WT and mutated B cells that express the same BCRs. For this

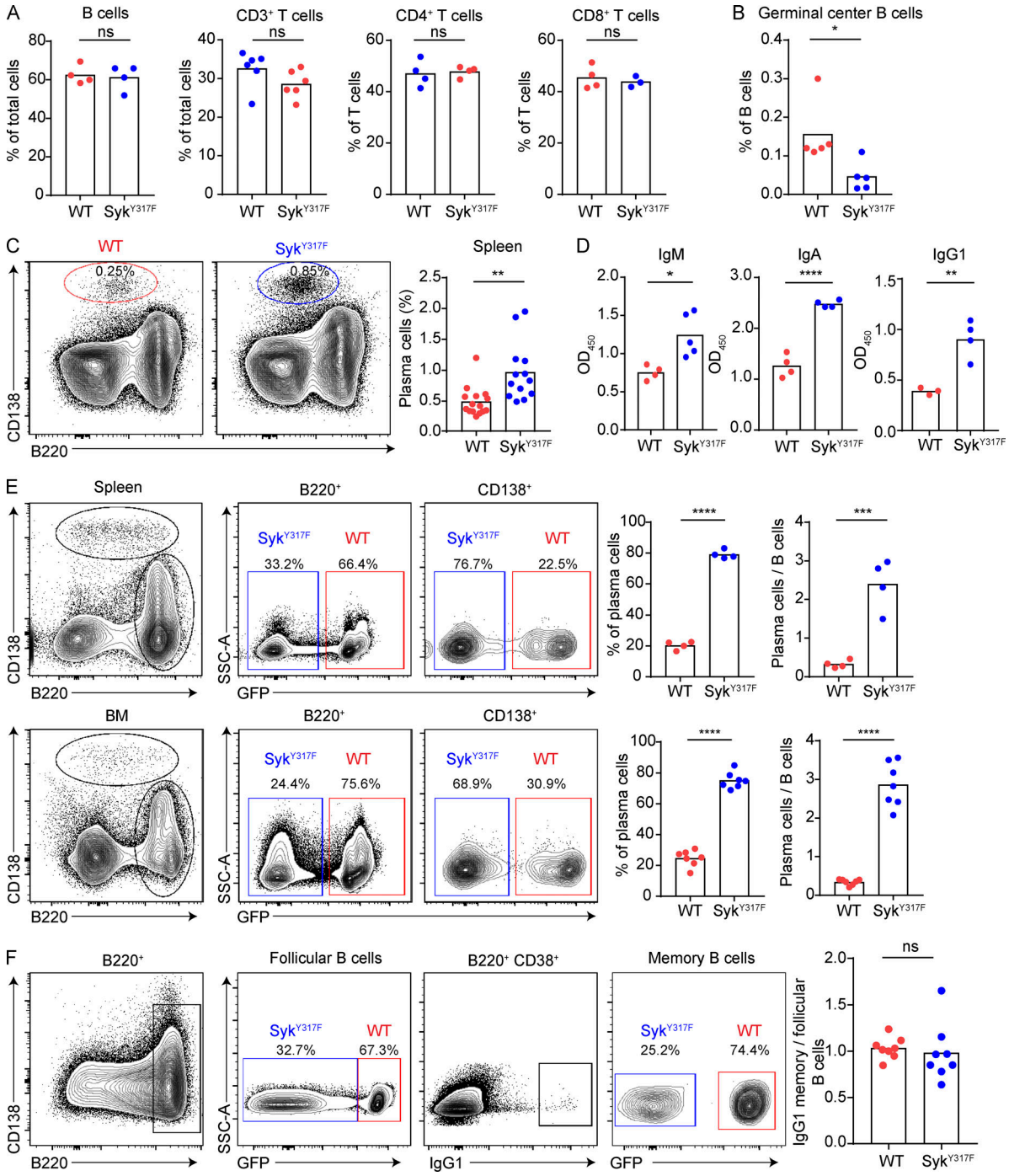

Figure 2. **SykY317F mice host high levels of PCs and show increased levels of serum immunoglobulins. (A)** Lymphocyte frequencies in the spleen of WT and SykY317F mice (n = 4 or 6, two independent experiments, two-tailed Student's t test). **(B and C)** Percentage of GC B cells (B220⁺ FAS⁺ CD38^{low}; B) and PCs (CD138⁺; C) in the spleen of unimmunized WT and SykY317F mice (n = 5, two independent experiments for B and n = 13, four independent experiments for C, two-tailed Student's t test). **(D)** Titers of total IgM, IgA, and IgG1 in serum of WT and SykY317F mice (n = 4 or 5, two independent experiments, two-tailed Student's t test). **(E)** Representative flow cytometry plots and quantification of CD138⁺ PC frequency and PC to B cell ratio in spleen and BM of chimeric hosts (n = 4, two independent experiments for spleen and n = 7, four independent experiments for BM, two-tailed Student's t test). **(F)** Quantification of CD38⁺ IgG1⁺ memory B cells in BM of chimeric mice (n = 8, two independent experiments, two-tailed Student's t test). Each dot in the graphs represents a single mouse; bars represent the mean. *, P = 0.05; **, P < 0.01; ****, P < 0.0001; ns, not significant; SSC-A, side scatter–area.

purpose, SykY317F mice were crossed with mice that express the B1-8^{hi} heavy chain gene. In these mice, B cells that express Igλ light chains (~15% of total B cells) form a BCR specific to the NP antigen (Shih et al., 2002a). A mixture of cells containing DsRed⁺ SykY317F B1-8^{hi} and control PA-GFP⁺ B1-8^{hi} B cells was transferred into host mice, followed by immunization with NP-OVA to the hind footpads. To increase the proportion of transferred cells in the GC and decrease variation in this experimental

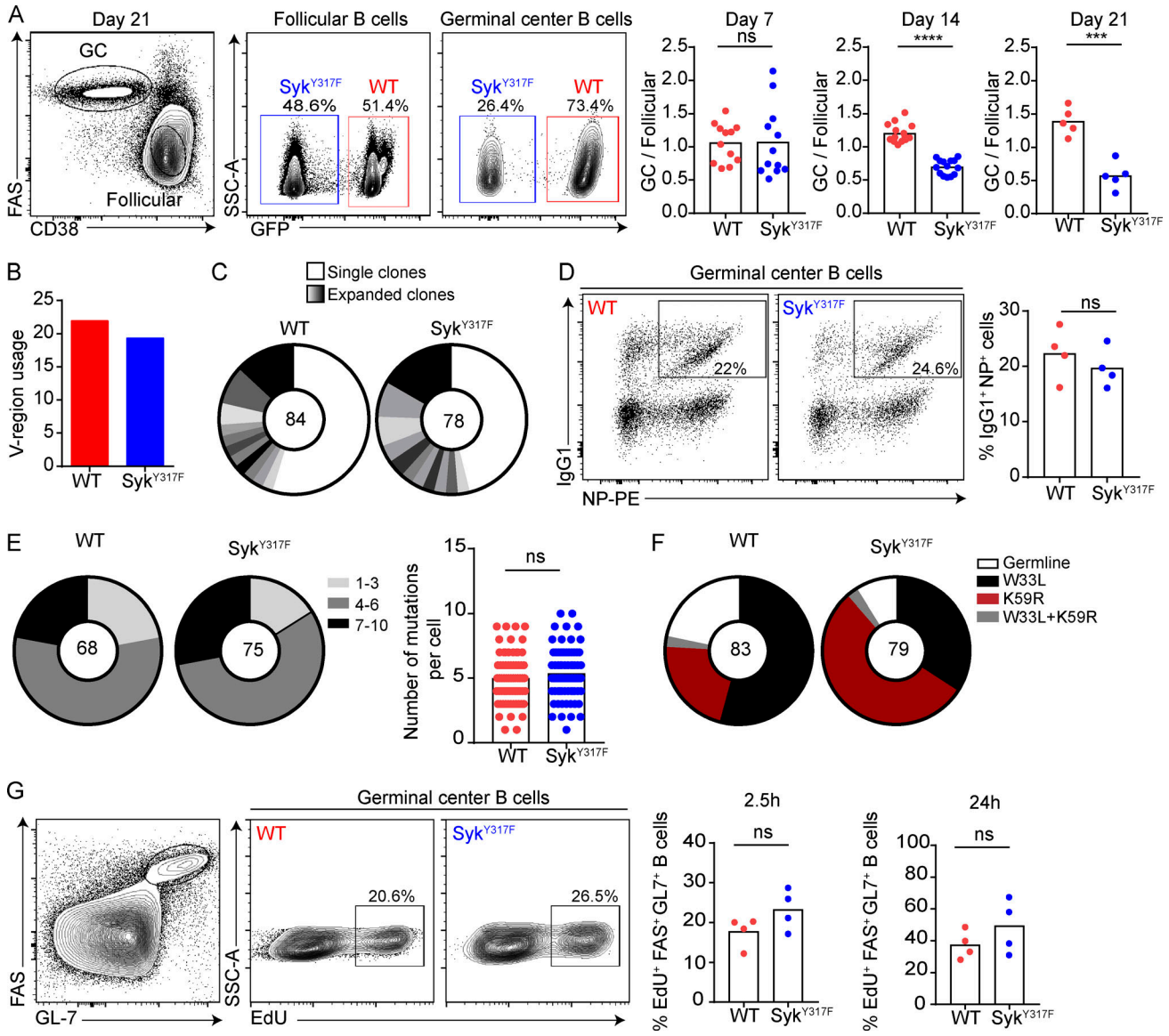

Figure 3. **Syk degradation is required for B cell retention in the GCs. (A)** Representative flow cytometry plots of GC cells ($B220^+$ FAS^+ $CD38^{low}$) and follicular B cells ($B220^+$ $CD38^{hi}$) in popliteal LNs of chimeric hosts, 7–21 d after immunization with NP-KLH. The graphs show the percentage of B cells in the GC normalized to the follicular B cell compartment (n = 12 for day 7, n = 14 for day 14, and n = 5 for day 21, two or three independent experiments, two-tailed Student's t test). **(B)** The number of V-regions detected in *Igh* sequences of GC B cells derived from one LN of a single chimeric mouse, 7 d after immunization. **(C)** Clonal distribution based on CD3 sequences as in B. **(D)** NP-specific $IgG1^+$ B cells in the GC of chimeric mice 7 d after immunization (n = 4, two independent experiments, two-tailed Student's t test). **(E)** The number of SHM in V_H186.2 genes of individual GC B cells (Igλ) that were sorted from WT and Syk^{Y317F} mice 21 d after immunization with NP-OVA. The total numbers of cells analyzed are indicated in the center of each pie chart. Graph shows quantification of the total number of SHM per single cell. Bars represent the mean of individual clones. **(F)** The frequency of single cells bearing W33L and K59R mutations in WT and Syk^{Y317F} mice 21 d after NP-OVA immunization. The number of single cells analyzed is indicated in the center of each chart. Each pie chart represents a pool of sequences derived from two mice. **(G)** Representative flow cytometry plots and quantification of $B220^+FAS^+GL7^+$ B cells 2.5 and 24 h after intravenous injection of EdU (n = 4, two independent experiments, two-tailed Student's t test). Each dot in the graphs represents a single mouse; bars represent the mean. ***, P < 0.001; ****, P < 0.0001; ns, not significant; SSC-A, side scatter–area.

setting, we used host mice in which most of the B cells express a BCR that binds hen egg lysozyme (MD4 mice) and cannot respond to the NP antigen. Flow-cytometric analysis of the different GC subpopulations, 7 d after immunization, revealed that both Syk^{Y317F} B1-8^{hi} and WT B cells entered the GC response to a roughly similar extent (Fig. S3 A). However, after an additional 7 d, the Syk^{Y317F} B1-8^{hi} were not detected in the GC cell population (Fig. S3 A). As observed in the polyclonal experiment (Fig. 3 G), we did not detect a significant difference in proliferation of transferred WT and Syk^{Y317F} B1-8^{hi} B cells by EdU staining (Fig. S3 B). Thus, we conclude that Syk degradation regulates GC persistence independently of variation in BCR specificity and relative affinity during GC seeding.

We further examined whether the reduction in Syk^{Y317F} B cells within GCs is a result of enhanced apoptosis. To this end, WT and Syk^{Y317F} B1-8^{hi} B cells were transferred into host mice,

and 7 d after immunization, B cells were stained with fluorescent Annexin V, which binds phosphatidylserine on membranes of apoptotic cells. Follicular B cells did not show significant binding of Annexin V, whereas control B cells that were subjected to apoptosis by heat shock showed high levels of Annexin V binding (Fig. S3 C). Analysis of GC cells did not reveal a significant difference in Annexin V staining between WT and Syk^{Y317F} B cells (Fig. S3 C). Thus, the reduction in the proportion of Syk^{Y317F} B cells cannot be explained by a significant increase in apoptosis within the GC compartment.

PC generation in GCs but not memory cell formation is attenuated by Syk degradation

Our initial analysis of Syk^{Y317F} mice revealed that they host high levels of PCs in their spleen and BM (Fig. 2 C). Furthermore, the increase in serum IgG1 levels indicated that antibody generation through a T cell–dependent response is enhanced in these mice (Fig. 2 D). Based on these observations, as well as the lack of measurable defects in other GC functions, we speculated that the reduced proportion of Syk^{Y317F} B cells in the GC compartment may be a result of enhanced differentiation of GC cells into PCs that contribute to the excess levels of T cell–dependent IgG1 antibodies in the serum. To interrogate this possibility, we examined the GC and PC compartments in lymph nodes of chimeric mice that were coreconstituted with WT and Syk^{Y317F} BM cells. Since the BM reconstitution efficiency varied between mice and experiments, we examined and present the frequency of follicular B cells, GC B cells, and PC of eight individual chimeric mice. 14 d after immunization with NP-KLH, we found that the proportion of WT B cells in the GC was higher compared with Syk^{Y317F} GC B cells; however, in all of the individual chimeric mice, regardless of BM reconstitution efficiency, the frequency of Syk^{Y317F} PCs was disproportionally higher compared with their percentage in the GC (Fig. 4 A). Normalization of the PC compartment to their corresponding subpopulations in the GC on day 14 after immunization revealed an increase in the proportions of Syk^{Y317F} PCs relative to their proportions in the GC compartment (Fig. 4 B). A similar analysis of CD38$^+$ IgG1$^+$ did not reveal an increase in the proportion of Syk ^{Y317F} memory B cells in immunized chimeric mice (Fig. 4 C). These findings suggest that Syk^{Y317F} GC B cells are more effective in generating PCs than their WT counterparts.

To evaluate whether these PCs depend on T cell functions for their formation at the specific time point of the analysis, we ablated the CD4$^+$ T cells during the peak of the GC response by injection of anti-CD4–depleting antibody to chimeric mice. This treatment resulted in nearly complete ablation of CD4 and GC cells in immunized mice (Fig. S3, D and E). Most importantly, depletion of CD4 T cells resulted in a considerable reduction in the number of PCs in the LN, demonstrating that these cells were recently formed in a T cell–dependent manner (Fig. 4 D and Fig. S3 F). These findings indicate that Syk degradation in B cells attenuates generation of PCs during the T cell–dependent immune response.

To examine specifically whether the CD138$^+$ population of Syk^{Y317F} B cells that was detected in lymph nodes by flow cytometry was indeed composed of GC-derived antibody forming cells, we used a pulse-chase approach that allows tracking of previously proliferating B cells in the GC reaction (Weisel et al., 2016; Li et al., 2018). Immunized chimeric mice were injected intravenously with EdU to label proliferating cells, and after 24 h, the proportions of EdU-positive cells within the PC compartment were examined by flow cytometry. We found that both WT and Syk^{Y317F} PCs were fluorescently labeled, suggesting that these cells divided within the GC compartment during the 24-h pulse period before the analysis (Fig. 4 E). Analysis of a shorter pulse of EdU (2.5 h) revealed that PCs rarely proliferate outside the GCs, and no enhanced EdU incorporation was observed in Syk^{Y317F} PCs (Fig. S4, A and B). Thus, these experiments confirm that WT and Syk^{Y317F} PCs of GC origin are formed in our experimental analysis. Collectively, we conclude that Syk degradation in GC B cells impedes PC formation.

We found that acquisition of mutations that enhance immunoglobulin affinity was not defective in the Syk GC B cells. Nonetheless, the enhanced generation of PCs during the GC response in Syk^{Y317F} mice predicts that serum antibody affinity would be reduced. To examine specifically serum antibody affinity, we immunized WT and Syk^{Y317F} mice and measured the amount of antigen-specific antibodies over time. ELISA for total NP-specific antibodies (NP_{20}) as well as for high-affinity antibodies (NP_4) revealed a small defect in antibody generation at a later time point during the immune response when the GC size is reduced (Fig. 4 F). Calculation of high-affinity versus total antibody ratio revealed that the affinity of the serum antibodies of the Syk^{Y317F} mice was constantly lower compared with the WT mice (Fig. 4 G). Together, we conclude that the increase in serum antibody affinity is less effective in Syk^{Y317F} mice.

Proper GC compartmentalization depends on Syk degradation

During the GC response, B cells iteratively migrate between the DZ, where they mutate their immunoglobulins and proliferate, and the LZ, where they interact with antigens and receive T cell–derived selection signals that further promote reentry into the DZ (Allen et al., 2007b; Victora and Nussenzweig, 2012). DZ B cells express high levels of CXCR4 and low levels of CD86, whereas LZ B cells show an inverse expression pattern (Victora et al., 2010; Allen et al., 2004). DZ to LZ ratio analysis revealed that these compartments were occupied almost normally by Syk^{Y317F} B cells in chimeric mice 7 d after immunization (Fig. 5 A); however, on day 14 and 21 after antigen challenge, when the proportion of the Syk^{Y317F} B cells in the GC was reduced, the DZ to LZ ratio of Syk^{Y317F} GC B cells was repeatedly skewed toward the LZ compartment (Fig. 5 B). These findings demonstrate that Syk degradation is required for effective persistence of B cells in the GC over time and acquisition of a DZ phenotype.

To further substantiate our conclusions, we took an alternative approach to study Syk functions by conditionally ablating Syk expression during the GC response. To this end, we crossed Syk$^{fl/fl}$ mice with mice expressing ERT2-Cre under the ubiquitin C promoter to produce a mouse strain wherein we can conditionally ablate Syk expression after GC formation. To specifically examine if Syk levels in B cells affect the DZ/LZ distribution in both WT and Syk^{Y317F} GC B cells, we generated mixed BM chimeric mice in which ∼50% of the B cells were derived from

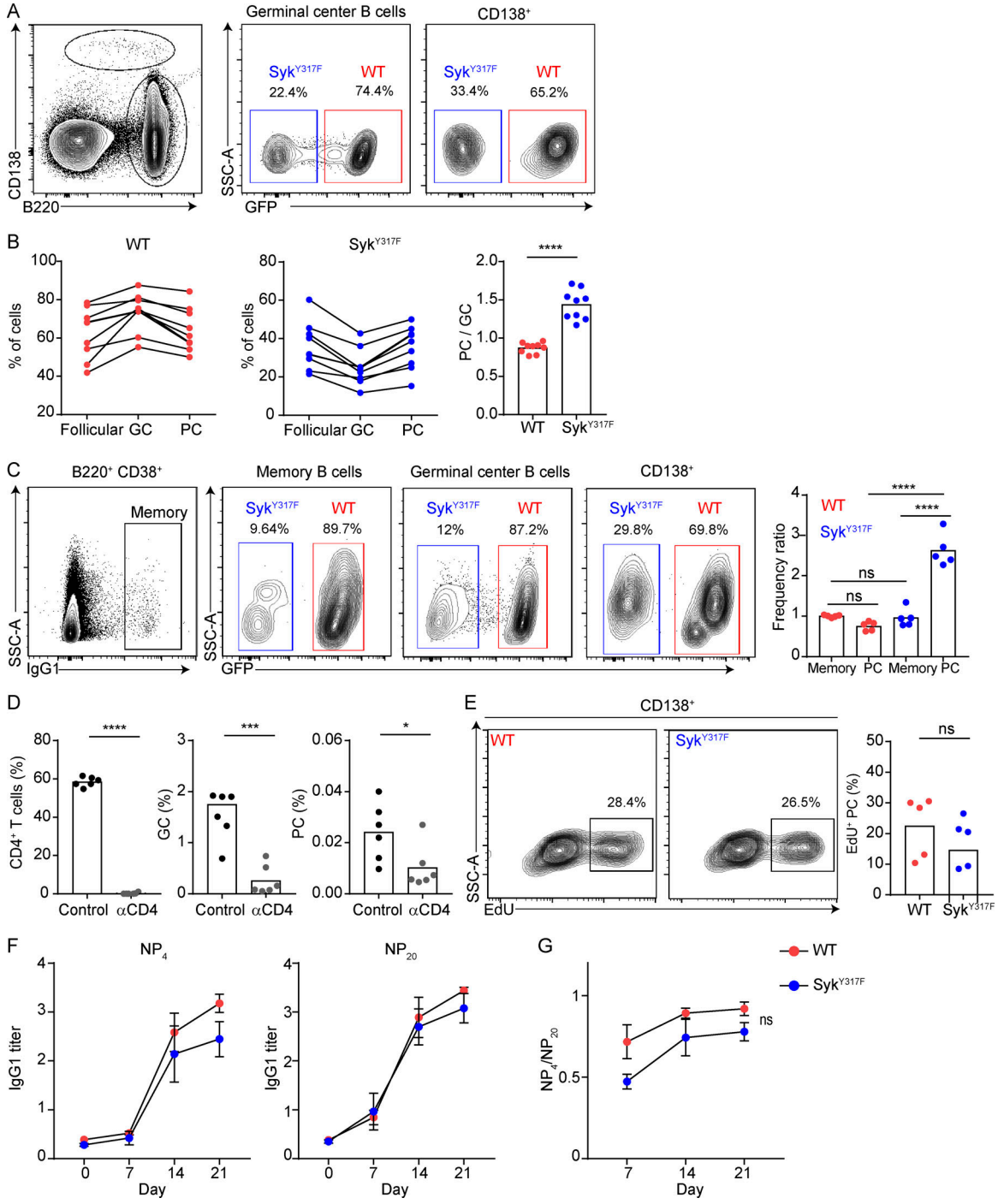

Figure 4. **PC formation in GCs is attenuated through Syk degradation. (A)** Representative flow cytometry plots of GC (B220$^+$ FAS$^+$ CD38^{low}) and PC (CD138$^+$) frequencies in popliteal LNs of chimeric hosts 14 d after immunization with NP-KLH. **(B)** Quantifications of follicular, GC, and PC compositions in individual WT and Syk^{Y317F} chimeric mice 14 d after immunization are shown. The bar graph shows analysis of GC to PC ratios in individual chimeric mice (n = 9, two independent experiments, two-tailed Student's t test). **(C)** Representative flow cytometry plots and quantification of memory (CD38$^+$ IgG1$^+$), GC, and PC ratios in immunized mice (n = 5, two independent experiments, two-tailed Student's t test). **(D)** Quantification of CD4$^+$ T cells, GC, and PC percentages following injection of CD4-depleting antibody or PBS to immunized mice. Gating strategy is shown in Fig. S3 (n = 6, two independent experiments, two-tailed Student's t test). **(E)** Representative flow cytometry plots and quantification of EdU$^+$ PCs 24 h after injection of EdU into mice 14 d after immunization (n = 0.5, two independent experiments, two-tailed Student's t test). Each dot in the graphs represents a single mouse; bars represent the mean. **(F)** Titers of total (NP_{20}) and high-affinity (NP_4) anti-NP IgG1 in the serum of NP-OVA immunized mice. **(G)** Ratios of high-affinity/total anti-NP antibodies. Lines represent the mean; error bars represent SEM (in F and G, n = 5–7, three independent experiments, two-tailed Student's t test). *, P = 0.05; ***, P < 0.001; ****, P < 0.0001; ns, not significant.

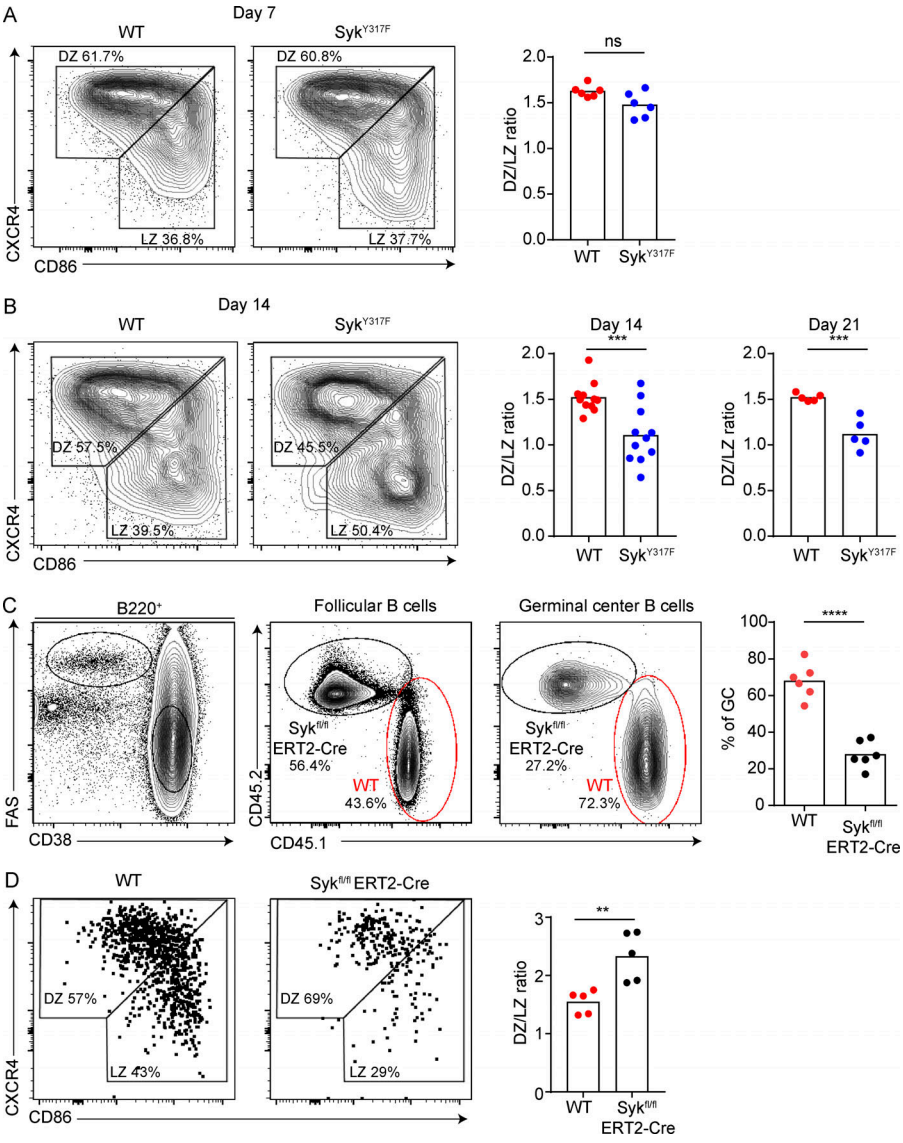

Figure 5. **Syk degradation regulates B cell interzonal transitions in GCs. (A and B)** Flow cytometry plots and graphs of DZ (CXCR4^{hi} CD86^{lo}) and LZ (CXCR4^{lo} CD86^{hi}) GC B cell distribution in chimeric mice 7 (A), 14, and 21 (B) days after immunization with NP-KLH (in A, n = 6, two independent experiments, two-tailed Student's t test; in B, n = 11 for day 14 and n = 5 for day 21, two or three independent experiments, two-tailed Student's t test). **(C)** Representative flow-cytometric analysis and quantification of WT (CD45.1) and Syk$^{fl/fl}$ ERT2-Cre (CD45.2) GC B cells in chimeric mice (~50% Syk$^{fl/fl}$ ERT2-Cre and ~50% WT). NP-KLH immunized mice were treated with tamoxifen at day 7 and analyzed at day 11 (two independent experiments with five mice total, two-tailed Student's t test). **(D)** DZ and LZ distribution in LNs of chimeric mice presented in C (n = 5, two independent experiments, two-tailed Student's t test). Each dot in the graphs represents a single mouse; bars represent the mean. **, P ≤ 0.01; ***, P < 0.001; ****, P < 0.0001; ns, not significant.

CD45.1$^+$ WT and ~50% were CD45.2$^+$ Syk$^{fl/fl}$ ERT2-Cre. Chimeric mice were treated with tamoxifen on day 7 after immunization with NP-KLH, when GCs were fully established, and the B cell subpopulations were examined 11 d after immunization. Flow-cytometric analysis of GCs in LNs of immunized mice revealed that the Syk$^{fl/fl}$ ERT2-Cre B cells were under-represented in the GC compartment (Fig. 5 C). Most importantly, analysis of the LZ and DZ compartments in the GC revealed that Syk-deficient B cells were enriched in the GC DZ compartment (Fig. 5 D). No difference in GC size and zonal distribution were observed between Syk$^{fl/fl}$ and Syk$^{fl/fl}$ ERT2-Cre–expressing mice that did not receive tamoxifen (Fig. S4, C and D). Together, these results complement our findings using Syk^{Y317F} mice and demonstrate that transition from DZ to LZ cellular state also depends on the expression of Syk.

Syk degradation regulates gene expression in LZ B cells and attenuates the Kras/Erk pathway

Our findings indicate that Syk plays a major role in B cell functions specifically in the LZ, where antigens are presented as immune complexes on FDCs (Heesters et al., 2014). To gain an additional insight regarding Syk activity in the different GC zones and in propagating downstream signals, LZ and DZ B cells were sorted from immunized chimeric mice, and their global gene expression was examined by mRNA sequencing. When comparing the transcriptome of DZ-derived WT versus Syk^{Y317F} B cells, we found that very few genes were differentially expressed (24 genes were significantly up-regulated, and 2 genes were down-regulated; Fig. 6, A–C), suggesting that Syk degradation plays only a minor role in regulating the transcriptome of the DZ cells. In sharp contrast, mRNA analysis of LZ cells revealed a massive change in gene expression of the Syk^{Y317F} B cells compared with WT B cells; 84 genes were significantly up-regulated and 363 genes were down-regulated in Syk^{Y317F} LZ B cells (Fig. 6, B and C). To identify signaling pathways that were changed in Syk^{Y317F} B cells, the gene signatures of LZ B cells were examined by gene set enrichment analysis (GSEA). This analysis revealed a significant change in the expression of genes that are associated with the Kras pathway (Fig. S5 A; Oh-hora et al., 2003;

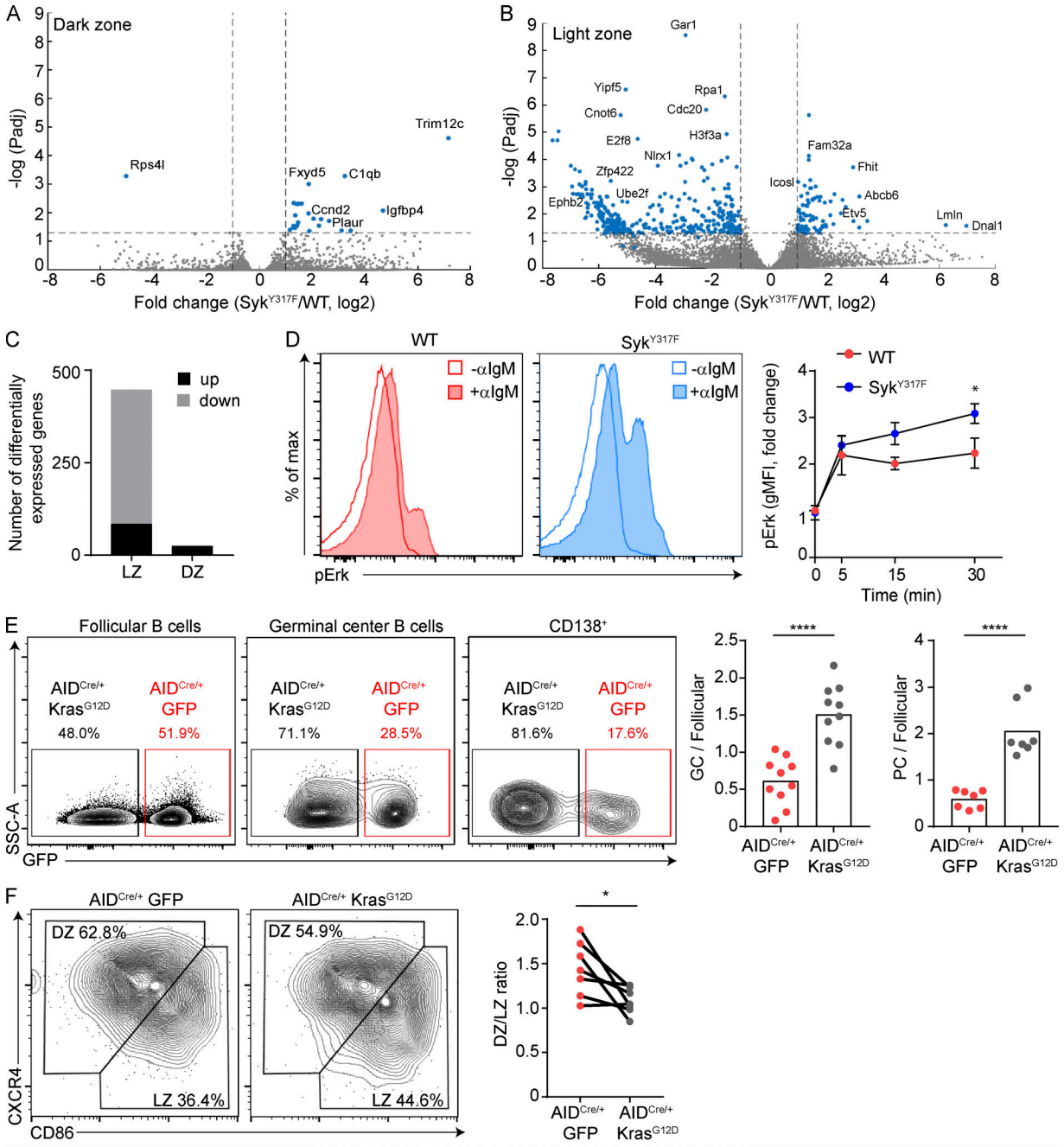

Figure 6. **Gene expression profiles in the LZ and the Kras/Erk pathway in GC B cells are regulated by Syk degradation. (A and B)** Volcano plots showing gene expression in DZ (CXCR4^{hi} CD86^{lo}; A) and LZ (CXCR4^{lo} CD86^{hi}; B) B cells, 14 d after immunization with NP-KLH. The x axis specifies the $\log_{(2)}$ of the fold-changes (FC), and the y axis shows the $\log_{(10)}$ of the p-adj values. Dotted horizontal and vertical lines indicate the filtering criteria (FC = ±1 and padj = 0.05). Blue dots represent differentially expressed genes. **(C)** Quantification of the differential significantly expressed genes in the LZ and DZ compartments of Syk^{Y317F} mice. The down-regulated genes in the LZ and the up-regulated genes in the DZ of Syk^{Y317F} mice were statistically significant, $P < 0.05$ (chi-square). **(D)** Flow-cytometric histograms and quantification of pErk in WT and Syk^{Y317F} B cells that were left unstimulated or stimulated with anti-IgM at different time points. Each graph represents the mean ± SEM ($n = 3$, three independent experiments, two-tailed Student's t test). **(E)** Representative flow cytometry plots of GC, PC, and follicular B cell composition in chimeric mice (~50% AID$^{Cre/+}$ GFP and ~50% AID$^{Cre/+}$ Rosa26$^{fl\text{-}stop\text{-}fl\ KrasG12D}$ B cells) 21 d after immunization with NP-KLH. The graph shows the percentage of B cells in the GC (B220$^+$FAS$^+$ CD38^{low}) normalized to the follicular B cell compartment (B220$^+$FAS$^-$CD38^{hi}; $n = 10$, three independent experiments for GC and $n = 7$, two independent experiments for PC, two-tailed Student's t test). **(F)** Flow cytometry plots and graphs of DZ and LZ distribution in individual chimeric mice as in E. Each line represents a single chimeric mouse ($n = 7$, two independent experiments, two-tailed Student's t test). In E and F, each dot represents a single mouse; bars represent mean. *, $P = 0.05$; ****, $P < 0.0001$. gMFI, geometric mean fluorescence intensity; p-adj, adjusted P value.

Kurosaki et al., 2010; Chen et al., 2016). In addition, changes in the PI3K pathway were also observed (Fig. S5 A). Thus, we conclude that Syk degradation regulates gene expression and modulates BCR downstream pathways primarily in the GC LZ, where the antigen is presented to B cells.

To verify if the Kras pathway is enhanced in Syk^{Y317F} B cells, we examined Erk phosphorylation in response to immunoglobulin stimulation in vitro. B cells were stimulated with anti-IgM for different time periods, followed by fixation and permeabilization for pErk intracellular staining. Flow-cytometric analysis revealed that in analogy to the prolonged calcium signaling in Syk^{Y317F} B cells (Fig. 1 E), the magnitude of Erk phosphorylation was higher in these cells compared with WT B cells (Fig. 6 D). These findings indicated that prolonged activation of Erk through the Kras pathway may promote some of the phenotypes observed in Syk^{Y317F} mice.

To determine whether the Kras/Erk pathway plays a role in maintaining the LZ state in GC in vivo, we crossed mice that express Cre under the activation-induced cytidine deaminase (AID) promoter to a mouse strain that carries a knock-in gene of a constitutively activated form of Kras in its Rosa26 locus ($Kras^{G12D}$; Jackson et al., 2001). In this model, continuous Kras activation occurs in GC B cells as well as in B cells that previously expressed AID, but not in the immature or naive B cell compartments. To examine how Kras activation affects B cell compartmentalization in the GC, we generated mixed BM chimeric mice from BM cells of control mice ($AID^{Cre/+}$ GFP), and mice described above ($AID^{Cre/+}$ $Kras^{G12D}$). Chimeric mice were immunized with NP-KLH, and the proportion of the two B cell types in the GC was examined after 21 d. Flow-cytometric analysis of GCs in the chimeric mice revealed that B cells expressing activated Kras were over-represented in the GC compartment compared with WT B cells (Fig. 6 E). Thus, constitutive Kras activation is sufficient to enhance GC occupancy. This outcome was different from the one observed in Syk^{Y317F} B cells, wherein BCR signaling intensity was increased only upon ligand-induced Syk activation. In contrast, in $Kras^{G12D}$ mice, signal propagation occurs constitutively regardless of immune receptor activation. Furthermore, in the chimeric mice, more PCs were produced from the cells that expressed activated Kras; however, it was impossible to assess if this observation was a result of enhanced signaling or enhanced GC occupation (Fig. 6 E). Most importantly, analysis of DZ and LZ distribution in individual chimeric mice revealed that enhanced Kras activation promoted the LZ phenotype in GC B cells, as was observed in Syk^{Y317F} B cells (Fig. 6 F). Thus, these experiments show that activation of the Kras pathway downstream of Syk partially phenocopies the skewed DZ/LZ segregation observed in the Syk^{Y317F} mice.

Syk degradation attenuates the PI3K/Foxo1 pathways and expression of PC transcription factors in follicular and GC B cells

Our gene expression analysis revealed that inhibition of Syk degradation affected the PI3K pathway (Fig. S5 A). Foxo1 is a master regulator of the DZ, and in its absence or when the PI3K pathway is over-activated, the GC contains only LZ B cells (Sander et al., 2015; Dominguez-Sola et al., 2015). BCR triggering leads to activation of the PI3K pathway and downstream activation of Akt as well as to deactivation of Foxo1 by phosphorylation (Kurosaki et al., 2010). To evaluate whether Syk degradation regulates the PI3K pathway, we stimulated B cells derived from WT and Syk^{Y317F} B cells with anti-IgM in vitro and examined Akt and Foxo1 phosphorylation by Western blot assay. This analysis revealed that the magnitude of phosphorylated Akt and Foxo1 was higher in Syk^{Y317F} B cells compared with WT B cells (Fig. 7, A and B). The steady-state levels of total Foxo1 were similar in WT and Syk^{Y317F} B cells (Fig. S5 B). We conclude that Syk degradation is required for attenuation of the PI3K pathway, and promotes Foxo1 activation by attenuating its phosphorylation.

To examine BCR signaling specifically in GC B cells, lymph nodes were removed from immunized mice, and cell suspensions were treated with anti-IgM and anti-IgG antibodies for 20 min followed by analysis of ribosomal protein S6 phosphorylation (p-S6), a target that is downstream of the BCR and PI3K/Akt pathway. We found that p-S6 was higher in Syk^{Y317F} B cells compared with WT B cells (Fig. 7 C). These results demonstrate that Syk degradation is required for attenuation of BCR signaling in GC B cells.

Previous studies established that the activation of Erks and PI3K enhances the generation of PCs by promoting expression of the PC transcription factors Irf4 and Blimp-1 (Yasuda et al., 2011; Shi et al., 2015; Setz et al., 2018). In addition, it was found that artificial activation of Syk promotes Blimp-1 expression in B cells; however, the role of Syk degradation in this process was not examined (Herzog et al., 2009). Furthermore, Blimp-1 repression activity antagonizes Bcl6 and extinguishes the GC program and in combination with high levels of Irf4 promotes PC differentiation (Ochiai et al., 2013; Nutt et al., 2015; Minnich et al., 2016). Based on these observations, we examined whether the prolonged BCR signaling and Erk activation in Syk^{Y317F} B cells lead to enhanced expression of PC transcription factors in vitro. Fresh follicular Syk^{Y317F} B cells did not show expression of Blimp-1 and Irf4 without stimulation (Fig. S5, C and D). In addition, both naive Syk^{Y317F} and WT B cells that were isolated from mouse spleens did not express Irf4 and Blimp-1 after 3 d in culture without activation signals (Fig. 7, D and E), demonstrating that Syk^{Y317F} B cells do not differentiate into PCs spontaneously. However, in response to anti-IgM stimulation, Syk^{Y317F} B cells showed enhanced Blimp-1 and Irf4 expression compared with WT cells (Fig. 7, D and E). To examine whether BCR triggering of Syk^{Y317F} B cells promotes expression of PC transcription factors more effectively in the GC compartment as well, we purified GC B cells from WT and Syk^{Y317F} mice that were immunized with NP-KLH and stimulated the cells with anti-IgM and anti-IgG for 16 h. We found that Syk^{Y317F} GC B cells expressed high levels of Blimp-1 and Irf4 in response to BCR stimulation compared with their WT counterparts (Fig. 7, F and G). Collectively, we conclude that Syk degradation in response to BCR triggering attenuates the Kras and PI3K pathways, and prevents excessive expression of PC transcription factors in antigen-engaged follicular and GC B cells.

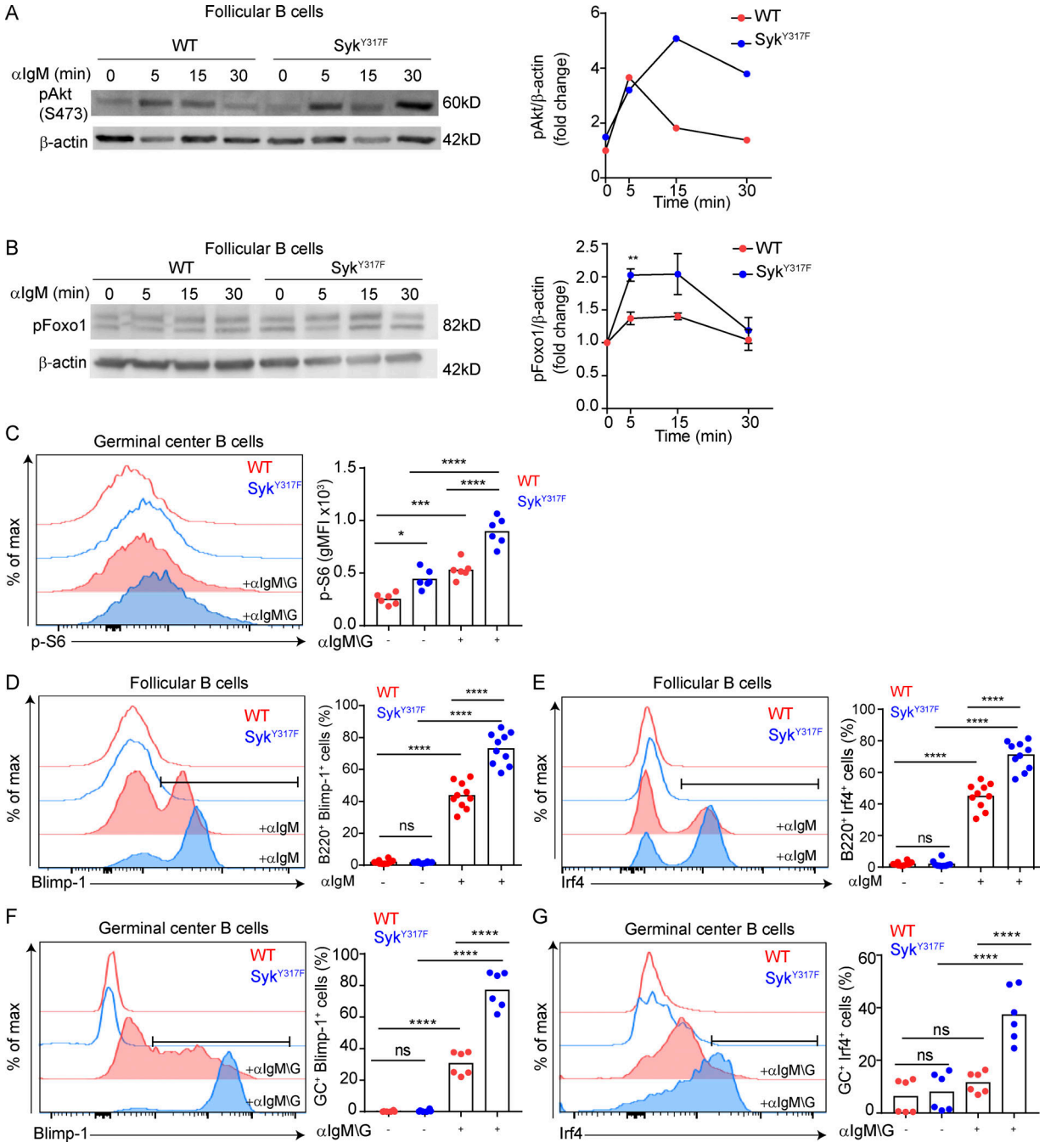

Figure 7. **The PI3K pathway and expression of PC transcription factors in follicular and GC B cells are attenuated by Syk degradation. (A and B)** pAkt (S473; A) and pFoxo1 (B) protein levels were determined by blot analysis of B cells that were stimulated with anti-IgM for the indicated time. Signals were normalized to β-actin and further normalized to unstimulated B cells at time 0, giving a value of 1. Blots shown are representative of two (pAkt) or three (pFoxo1) independent experiments. Data were analyzed using the two-tailed Student's *t* test. **(C)** Cells derived from WT and Syk^{Y317F} mice 14 d after NP-KLH immunization were kept unstimulated or stimulated with anti-IgM and anti-IgG antibodies for 20 min. Quantifications of p-S6 in GC B cells (B220$^+$ FAS$^+$ CD38^{low}) are shown. Each dot in the graphs represents a single repetition in vitro (n = 6, two independent experiments, one-way ANOVA). **(D and E)** Flow cytometry histograms and quantification of the expression of Blimp-1 (D), and Irf4 (E) in response to anti-IgM stimulation of follicular B cells for 3 d (n = 10, two independent experiments, one-way ANOVA). **(F and G)** Expression of Blimp-1 (F) and Irf4 (G) in GC B cells that were kept unstimulated or stimulated for 16 h with anti-IgM and anti-IgG (n = 6, two independent experiments, one-way ANOVA). In C–G, each dot in the graphs represents a single repetition in vitro. *, P = 0.05; **, P ≤ 0.01; ***, P < 0.001; ****, P < 0.0001; ns, not significant.

Discussion

The major purpose of the GC reaction is to generate memory B cells and PCs that secrete high-affinity antibodies and provide long-lasting protection from previously encountered pathogens. Here, we describe a novel molecular mechanism of BCR signal transduction that controls the balance between PC formation and GC retention. We find that extended BCR signaling through Syk supports the formation of PCs, whereas progressive Syk

degradation attenuates and limits the duration of the signal transduction and thereby promotes B cell transition into a DZ cell state.

Based on measurements of calcium signaling induced in response to BCR ligation in Cbl-deficient B cells, previous studies concluded that Cbl plays a role as a negative regulator of BCR signaling (Sohn et al., 2003); however, so far, a direct connection between Cbl and BCR signaling was not established. Thus, it seems that the BCR regulates the degradation events of specific downstream factors rather than directly controlling Cbl functions (Ise and Kurosaki, 2019). We find that inhibition of Cbl-mediated Syk degradation is sufficient to replicate the negative outcome of Cbl deletion in B cells (Lupher et al., 1998; Rao et al., 2002), suggesting that the Cbl-dependent attenuation of BCR activation functions specifically through this molecular mechanism. A recent study demonstrated that Cbl prevents premature PC differentiation by ubiquitylation and degradation of Irf4 and Cbl itself (Li et al., 2018). Our study adds an additional and specific Cbl-mediated mechanism in proximity to the BCR that suppresses the expression of PC transcription factors. Thus, post-translational mechanisms that regulate degradation events of proximal and distal BCR downstream signals, as well as negative feedback loops by phosphorylation and dephosphorylation events, attenuate BCR signaling and suppress PC generation (Li et al., 2018; Shlomchik et al., 2019; Guo et al., 2019).

During the GC response, B cells proliferate and insert mutations into their immunoglobulin genes followed by antigen engagements and interactions with T cells in the LZ (Victora and Nussenzweig, 2012). Whereas BCR signaling plays a key role throughout the B cell response, our findings demonstrate that BCR-induced Syk degradation in vivo primarily regulates B cell functions after GC formation. This suggests that regulation of BCR signal transduction through Syk decay plays a more significant role when the B cells are subjected to a selective pressure, i.e., when the antigen is a limiting factor, and some of the cells acquire affinity-enhancing mutations. B cell transition from the LZ to the DZ requires T cell help and depends on the expression of Myc and Foxo1, the transcription factor that regulates the DZ program (Sander et al., 2012; Dominguez-Sola et al., 2012, 2015; Sander et al., 2015). Transient inhibition of LZ to DZ transition through BCR signaling and Foxo1 inactivation is expected to increase B cell encounters with T cells that promote the expression of Myc (Biram et al., 2019; Luo et al., 2018). A concomitant decline in Foxo1 constraining signals through BCR signaling attenuation, coupled to Foxo1 and Myc transcription, may optimally promote B cell transition to the DZ (Luo et al., 2019). Thus, we suggest that initial positive BCR signals followed by long lasting signal transduction desensitization through degradation events and negative feedback loops promote T cell–dependent entry to the DZ. Nonetheless, since the BCR signal is expected to become weaker over time, and since enhanced B cell signaling through Syk did not endow GC B cells with preferential advantage in clonal expansion, it seems that selection of the high-affinity variants for enhanced proliferation in the DZ is mediated by antigen uptake and presentation to T cells (Gitlin et al., 2014, 2015; Kwak et al., 2018). In contrast, enhanced BCR signaling through Syk favors B cell differentiation into PCs.

In the DZ, Foxo1 is highly expressed (Sander et al., 2015; Dominguez-Sola et al., 2015), and since most of the antigen is not retained in this compartment, BCR signaling is not expected to induce Foxo1 inactivation by phosphorylation in this zone. Therefore, there is no need for negative regulation by degradation of proximal BCR signals in the DZ. This conclusion is further supported by the finding that Cbl is expressed primarily in the GC LZ (Li et al., 2018) and by our transcriptomic analyses that revealed only minor differences in gene expression between WT and Syk^{Y317F} B cells in the DZ. Thus, we conclude that the regulation of BCR signal transduction by Syk degradation is a specialized mechanism associated with the GC LZ, where interactions with antigens and affinity-based selection by T cells take place.

BCR triggering induces numerous phosphorylation events that propagate downstream signals, followed by rapid desensitization of the signaling pathways through phosphatase activity (Geahlen, 2009; Luo et al., 2019). As opposed to phosphorylation and dephosphorylation events that are transient and can be rapidly reversed, replenishment of Syk protein levels after its degradation in the LZ depends on gene expression. Thus, the major difference between these two desensitization mechanisms is the time scale of the signal transduction recovery. It is possible that the phosphorylation of proximal BCR signals followed by dephosphorylating events allow the cells to serially engage with antigen over time, while Syk decay is a process with a long-lasting effect on cell fate. During the GC reaction, B cells interact with a limiting amount of antigen that is deposited as immune complexes on FDCs, found in the GC LZ (Heesters et al., 2014). As opposed to initial priming of B cells, most of the cognate interactions in the GC are very short-lived (~3 min), suggesting that the BCR of GC B cells is triggered sequentially as the cells migrate over the FDC network (Schwickert et al., 2007; Suzuki et al., 2009). Based on these early observations and our new findings, we suggest that Syk is constantly subjected to transient phosphorylation events in parallel to a progressive decrease in Syk protein levels by degradation. The level of Syk might serve as a decay timer that initially favors LZ retention, when the amount of Syk is high within the cells, while the progressive reduction in Syk levels as a result of its gradual degradation may favor transition from the LZ to the DZ state. Furthermore, based on Syk deletion experiments performed by us and others (Luo et al., 2018), it seems that Syk reexpression in the DZ, among other factors, is required for B cell transition into an LZ cell state, possibly through replenishment of BCR tonic signaling. Collectively, we conclude that Syk is an important regulator of the cyclic reentry process in GCs.

It was previously shown that activation of the Kras downstream effectors, Erk1/2, leads to phosphorylation and degradation of the GC master regulator, Bcl6 (Niu et al., 1998), and indeed it was demonstrated that a transitional B cell population in the GC expresses less Bcl6 at the protein level (Basso and Dalla-Favera, 2015; De Silva et al., 2016; Laidlaw et al., 2017; Ise et al., 2018). Erk proteins are essential for PC differentiation by regulating the expression of Irf4 and Blimp-1 (Yasuda et al., 2011) through phosphorylation of Pax5, a repressor of Blimp-1

expression (Yasuda et al., 2012). Furthermore, expression of Blimp-1 that promotes PC generation in GCs depends on high expression of Irf4 levels (Sciammas et al., 2006; Ochiai et al., 2013), and indeed, rare B cells that recently interacted with antigen express Irf4 and Blimp-1 in the LZ (Mueller et al., 2015). Thus, Syk degradation may modulate the expression of Bcl6 and Blimp-1 through the Kras/Erk pathway and thereby may regulate the balance between GC retention and PC generation.

In summary, we describe here how progressive degradation of a key signaling molecule controls the magnitude and duration of receptor signaling and changes the fate of immune cells. It is most likely that the tight control on BCR signaling through Syk degradation and phosphatase-based mechanisms play a key role in preventing the emergence of autoimmune diseases, and its regulatory components may serve as targets for treatment of patients (Deng et al., 2016). Furthermore, since Syk-dependent signaling cascades promote tumorigenesis in lymphoid cells, this molecular mechanism can serve as a target to enhance Syk degradation in acute lymphoblastic leukemia cells that depend on Syk activity for their survival (Perova et al., 2014).

Materials and methods

Mice

$AID^{Cre/+}$, UBC-CreERT2, SJL $CD45.1^+$, PAGFP, GFP, MD4, OT-II, DsRed-expressing mice, $Syk^{fl/fl}$, and $Rosa26^{fl\text{-}stop\text{-}fl\ KrasG12D}$ mice were purchased from the Jackson Laboratory. NP-specific B1-8^{hi} mice (Shih et al., 2002b) were a gift from M. Nussenzweig (The Rockefeller University, New York, NY). Syk^{Y317F} mice were generated as described below. WT mice (C57BL/6) were provided by Harlan. All experiments using mice were approved by the Weizmann Institute Animal Care and Use Committee.

CRISPR/Cas9 generation of Syk^{Y317F} mice

Cas9 plasmid and plasmids encoding guide RNAs were generated in our laboratory. The following oligos were used for construction of guide RNA vectors: Syk_F1 5′-TAATACGACTCACTATAGGACCCCTATGAGCCAACGGGAGTTTTAGAGCTAGAAAT-3′ and Syk_R2 5′-ATTTCTAGCTCTAAAACTCCCGTTGGCTCATAGGGGTCCTATAGTGAGTCGTATTA-3′. In vitro transcribed Cas9 RNA (100 ng μl^{-1}) and guide RNA (50 ng μl^{-1}) were injected into one-cell fertilized embryos isolated from superovulated C57BL/6 hybrid mice mated with males (Harlan Biotech Israel). Injected embryos were transferred into the oviducts of pseudopregnant ICR females as previously described (Wang et al., 2013).

Adoptive cell transfer

B cells and T cells were purified by forcing spleen tissue through mesh into PBS or RPMI containing 2% serum and 1 mM EDTA. Resting B cells and T cells were purified using anti-CD43 magnetic beads or $CD4^+$ T cell–negative isolation kits (Miltenyi Biotec), respectively. After purification, 2–4 × 10^6 B1-8^{hi} B cells were transferred intravenously into host mice before immunization. In experiments wherein B1-8^{hi} B cells were transferred into WT mice, 0.5 × 10^6 OT-II T cells were cotransferred. In competition experiments, the ratio of adoptively transferred cells was 50:50.

Chimeric mice

For generation of chimeric mice, WT hosts were irradiated with 950 rad and injected intravenously with BM cells derived from various donor mice. In Fig. 2, Fig. 3 A, Fig. 4, and Fig. 5, mice were reconstituted with 30–50% Syk^{Y317F} and 20–50% CD45.1 or GFP WT BM cells. In Fig. 5, C and D, mice were reconstituted with 50% $Syk^{fl/fl}$ ERT2-Cre and 50% CD45.1 WT BM cells. In Fig. 6, E and F, mice were reconstituted with 50% $AID^{Cre/+}$ $Rosa26^{fl\text{-}stop\text{-}fl}$ $Kras^{G12D}$ and 50% SJL or $AID^{Cre/+}$ GFP BM cells. Mice were used 8–16 wk after BM reconstitution.

Immunization and treatments

Mice were injected with 25 µl PBS containing 10 µg NP_{31}-KLH in alum into the hind footpads. In experiments involving cell transfer, mice were injected with 10 µg NP_{16}-OVA precipitated in alum into the hind footpads. Cre-mediated deletion of Syk was triggered by tamoxifen administration (Sigma-Aldrich, 15 mg/mouse) by oral gavage on day 7 after immunization. For CD4 blocking after primary immunization, mice were injected with CD4 blocking antibody (GK1.5, Bio-X-Cell) or PBS administered both intravenously (200 µg) and into hind footpads (10 µg) 10 d after immunization.

Flow cytometry

Single-cell suspensions were obtained by forcing popliteal lymph nodes through mesh into PBS or RPMI containing 2% serum and 1 mM EDTA. Cells were incubated with 2 µg/ml anti-16/32 (clone 93) for blockage of Fc receptors for 5–10 min. Cell suspensions were washed and incubated with fluorescently labeled antibodies (Table S1) for 20–40 min. GC cells were gated as live/single, $B220^+CD38^{low}$ FAS^+. Early activated B cells on day 3 after immunization and PCs were defined as $GL\text{-}7^+$ FAS^+ and $B220^{med}$ $CD138^+$, respectively. For detection of B cells in chimeric mice, cell suspensions were stained for GCs ($CD38^{low}$ FAS^+), CD45.1, and CD45.2. For intracellular staining, cells were permeabilized using the Foxp3/Transcription factor-staining buffer set (eBioscience). Apoptosis was quantified by staining the cells with Alexa Fluor 647–conjugated Annexin V. For in vivo proliferation analysis, mice were injected intravenously and in the hind footpad with 2 mg and 0.25 mg EdU (Invitrogen), respectively, in PBS. Cells were then stained for surface antigens as described above and processed using Click-iT EdU-488 or 647 (Molecular Probes) according to the manufacturer's protocols. For intracellular calcium analysis, splenocytes were loaded with 2 µM Indo-1 acetoxymethyl (Indo-1 AM, Invitrogen) in $PBS^{+/+}$ containing 0.5% BSA at 37°C for 30 min. After loading, cells were washed and stained with B220-A780 (eBioscience). Cells were washed and resuspended in $PBS^{+/+}$/0.5% BSA. After a baseline was established, cells were stimulated with 1 or 10 µg/ml $F(ab')_2$ anti-mouse IgM (Jackson ImmunoResearch) and immediately analyzed for 10 min by flow cytometry using an LSRII flow cytometer. Intracellular calcium levels were determined by measurement of the fluorescence ratio of 440/40 nm to 530/30 nm emissions (violet to

blue ratio). The amount of NP-specific B cells was quantified by staining the cells with NP-PE.

Stimulation of naive B cells in vitro

Spleens from WT and Syk^{Y317F} mice were processed by forcing spleen tissue through mesh into PBS. Cells were seeded at 10^6/ml, and then incubated at 37°C in B cell medium (RPMI-1640 medium supplemented with 10% FBS, penicillin/streptomycin, gentamycin, glutamine, pyruvate, nonessential amino acids, and 50 µM β-mercaptoethanol) with or without stimulation for various times as indicated in the figure legends. For CD86 up-regulation, spleen cells were stimulated with anti-IgM (10 µg/ml) for 16 h, and for Blimp-1 and Irf4 expression, purified CD45.2$^+$ B cells were stimulated with anti-IgM (10 µg/ml) for 3 d in the presence of CD45.1$^+$-supporting spleen cells. B cells were stained with the indicated antibodies and analyzed by flow cytometry, and CD45.1$^+$ cells were gated out from the analysis. For pErk and pSyk analysis, cells were incubated with anti-IgM (10 µg/ml) for the indicated time periods. The reaction was stopped by adding paraformaldehyde to a 1.5% final concentration followed by incubation for 10 min at room temperature. Fixed cells were then permeabilized with ice-cold methanol and incubated for 10 min at 4°C. Cells were washed twice with PBS 1% BSA to remove residual methanol. Samples were then incubated with anti-B220 and pErk or pSyk antibodies for 30 min at 4°C. FACS analysis was performed as described below.

Stimulation of GC-derived B cells

Splenic B cells were purified from WT and Syk^{Y317F} mice 14 d after NP-KLH intraperitoneal immunization using CD43 magnetic beads. Purified B cells were incubated with PE-conjugated IgD and CD38 antibodies followed by magnetic bead depletion of labeled cells with anti-PE beads (Miltenyi Biotec). The enriched cell population contained ∼80% GC B cells. These cells were incubated in B cell medium and stimulated with 10 µg/ml anti-IgM, 10 µg/ml biotinylated anti-IgG, and 1 µg streptavidin (Jackson ImmunoResearch) at 37°C for 16 h. For the p-S6 experiment, WT and Syk^{Y317F} mice were intradermally immunized with NP-KLH in CFA for 12 d. Spleen-derived cells were warmed to 37°C with 5% CO_2 in medium for 30 min. After the incubation, 20 µg/ml biotinylated anti-IgG was added for 5 min followed by streptavidin cross-linking and anti-IgM stimulation (10 µg/ml) for an additional 20 min.

Western blot analysis

Naive splenic B cells were isolated using anti-CD43 magnetic beads (Miltenyi Biotec). Purified B cells were kept unstimulated, or stimulated with anti-IgM (10 µg/ml) for the indicated time periods at 37°C. The cells were then lysed in radioimmunoprecipitation assay buffer (50 mM Tris, 150 mM NaCl, 1% NP-40, 0.5% deoxycholate, protease inhibitors, and phosphatase inhibitors). Lysates were centrifuged for 15 min at 20,000 *g* at 4°C. Cleared lysates were boiled with SDS reducing sample buffer for 5 min, separated by SDS-PAGE (Bio-Rad), and transferred to nitrocellulose membranes. Blots were blocked with 5% skim milk in Tris-buffered saline + 0.1% Tween for 1 h at room temperature and incubated with specific primary antibodies overnight at 4°C with gentle agitation. The following antibodies were used for biochemical studies: anti-Syk (clone: 5F5, Biolegend); anti-pFoxo1 (polyclonal, Cell Signaling Technology), anti-Foxo1 (clone: C29H4, Cell Signaling Technology), anti-pAkt (clone D9E, Cell Signaling Technology), anti-β-actin (clone: BA3R, Thermo Fisher Scientific) and anti-GAPDH (clone: 6C5, Merck Millipore). Horseradish peroxidase–conjugated donkey anti-mouse or anti-rabbit secondary antibodies (Jackson ImmunoResearch) and ECL Reagent (Biological Industries) were used for detection.

Analysis of BCR internalization by flow cytometry

B cells were incubated with biotin–anti-mouse IgM (10 µg/ml, Biolegend) at 4°C for initial BCR binding and then incubated at 37°C for 0, 5, 10, and 30 min. Biotin–F(ab′)$_2$–anti-IgM remaining on the cell surface after the incubation was stained with APC-streptavidin and quantified using flow cytometry. The data were expressed as percentages of the cell surface–associated biotin–anti-IgM antibody at time 0 (Sharma et al., 2009).

ELISA

Serum was collected from unimmunized mice, and IgM, IgA, and IgG1 antibodies in the serum were detected by ELISA using anti-mouse IgM, IgA, and IgG1–horseradish peroxidase, respectively. For antibody affinity maturation analysis, WT and Syk^{Y317F} mice were immunized intraperitoneally with 100 µg NP-OVA in alum. Serum was collected from mice every 7 d. NP-specific antibodies in serum were quantified by ELISA with NP_4-BSA or NP_{20}-BSA that was coated on 96-well plates. NP-specific IgG1 in serum of immunized mice was detected using anti-mouse IgG1–horseradish peroxidase.

Single-cell immunoglobulin analysis

Popliteal lymph nodes from immunized mice were harvested and processed for flow cytometry analysis. Cells were sorted using a FACS Aria cell sorter (BD Bioscience) into 96-well plates containing lysis buffer (PBS containing 3 U/µl RNAsin and 10 mM dithiothreitol). cDNA was purified using random primers (NEB) as previously described (von Boehmer et al., 2016).

For chimeric mice (50% Syk^{Y317F} and 50% GFP) analysis, cell suspensions were stained for dump (CD4, CD8, GR-1, F4/80) and gated as dump$^-$ B220$^+$ Fas$^+$GL7$^+$IgG1$^+$GFP$^+$ or dump$^-$ B220$^+$ Fas$^+$ GL7$^+$IgG1$^+$GFP$^-$ representing WT and Syk^{Y317F} GC B cells, respectively. Igγ1 heavy-chain sequence was amplified twice using primers for the Igγ1 constant region (5′-GGAAGGTGTGCACAC CGCTGGAC-3′ in the first reaction and 5′-GCTCAGGGAAATAGC CCTTGAC-3′ in the second reaction) together with a mix of primers for the variable regions (Table S2; Ho et al., 2016).

For WT and Syk^{Y317F} VH186.2 sequence analysis, cell suspensions were gated as dump$^-$ B220$^+$CD138$^-$ GL-7$^+$FAS$^+$ Igλ$^+$ IgG1$^+$. Nested PCR was used to amplify VH186.2 segment of Igγ1 heavy chains. NP-specific VH186.2 Igγ1 clones were amplified using the primers: VH186.2 (5′-CTAGTAGCAACTGCAACCGGT GTACATTCTCAGGTGCAGCTGCAGGAGTC-3′) and Igγ1 outer (5′-GGAAGGTGTGCACACCGCTGGAC-3′) followed by a second reaction with the VH186.2 and Igγ1 inner primers (5′-GCTCAG GGAAATAGCCCTTGAC-3′). For total V(D)J sequencing of Igγ1

heavy chains, the sequences were amplified by nested PCR using primers for the Igγ1 constant region (5′-GGAAGGTGTGCACAC CGCTGGAC-3′ for the first reaction and 5′-GCTCAGGGAAAT AGCCCTTGAC-3′ for the second reaction) together with a mix of primers for the variable regions.

For both experiments, the PCR products were sequenced and analyzed for CDR3 using web-based IgBlast and IMGT tools. Sequence alignment was performed using SnapGene software (GSL Biotech). Primer-derived mutations were excluded from the analysis.

RNA sequencing and transcriptome analysis

Popliteal lymph nodes from immunized mice were harvested from chimeric mice (50% Syk^{Y317F} and 50% GFP) and processed for flow cytometry analysis. Cell suspensions were stained for $dump^-$ (CD4, CD8, GR-1, F4/80) and $B220^+$ $CD138^-$ $GL\text{-}7^+$ FAS^+ $CXCR4^+$ $CD86^-$, or $B220^+$ $CD138^-$ $GL\text{-}7^+$ FAS^+CXCR4^- $CD86^+$ populations, representing DZ cells or LZ cells, respectively. Cell sorting was performed using a FACS Aria cell sorter (BD Bioscience). For gene expression analysis, 1–3 × 10^3 cells from each population were sorted into 50 µl of lysis/binding buffer (Life Technologies). mRNA was captured with 12 ml of oligo(dT) Dynabeads (Life Technologies), washed, and eluted at 85°C with 10 µl of 10 mM Tris-Cl (pH 7.5). A variation of MARS-seq was used as described (Jaitin et al., 2014), developed for single-cell RNA sequencing to produce expression libraries with a minimum of two replicates per population.

MARS-seq analysis was done using the UTAP transcriptome analysis pipeline (Kohen et al., 2019) of the Weizmann Institute Bioinformatics Unit. Reads were trimmed using Cutadapt and mapped to the Mus_musculus genome (UCSC mm10) using STAR (Dobin et al., 2013) v2.4.2a with default parameters. The pipeline quantifies the genes annotated in RefSeq (extended by 1,000 bases toward the 5′ edge and 100 bases in the 3′ direction). Counting of sequenced reads was done using htseq-count (Anders et al., 2015; union mode). Genes having minimum of five UMI-corrected reads in at least one sample were considered. Normalization of the counts and differential expression analysis was performed using DESeq2 (Love et al., 2014) with the following parameters: betaPrior = True, cooksCutoff = FALSE, independentFiltering = FALSE. Raw P values were adjusted for multiple testing using the procedure of Benjamini and Hochberg. The threshold for significant differential expression was: padj ≤ 0.05, |log2FoldChange| ≥ 1 and baseMean ≥ 5.

The data discussed in this publication have been deposited in the National Center for Biotechnology Information's Gene Expression Omnibus (Edgar et al., 2002) and are accessible through Gene Expression Omnibus series accession no. GSE140282.

GSEA was performed using GSEA 3.0 with the GSEAPreranked tool (Subramanian et al., 2005; Mootha et al., 2003). Gene names were converted to human gene symbols, and ran with default parameters. The Molecular Signature Database hallmark gene sets were used to perform pathway enrichment analysis using a hypergeometric distribution and limiting the output to the top 100 gene sets.

Statistical analysis

Statistical significance was determined with GraphPad Prism Version 5.0 using the tests indicated in each figure.

Online supplemental material

Fig. S1 shows IgM and IgG1 expression and Syk phosphorylation at Y348 of WT and Syk^{Y317F} mice. Fig. S2 shows WT and Syk^{Y317F} B cell developmental stages in the BM, peripheral blood, and spleen. Fig. S3 shows the persistence of B1-8^{hi} and B1-8^{hi} Syk^{Y317F} B cells in the GC. Fig. S4 shows EdU incorporation in WT and Syk^{Y317F} PCs and the ERT2-Cre effect on the GC reaction without tamoxifen. Fig. S5 shows the expression of Kras and PI3K target genes and Foxo1, Blimp-1, and Irf4 levels in WT and Syk^{Y317F} mice without stimulation.

Acknowledgments

We thank Dr. Gabriel Victora for valuable comments and discussions. We thank Dr. Hadas Keren-Shaul from the Sandbox unit in the Life Science Core Facility of the Weizmann Institute of Science for guidance and critical advice regarding sequencing.

Z. Shulman is supported by European Research Council grant no. 677713, the Israel Science Foundation (2759/19), and the German Israeli Foundation for Scientific Research and Development (2506). Z. Shulman is a member of the European Molecular Biology Organization Young Investigator Program, and also supported by the Human Frontiers of Science Program (CDA-00023/2016), Azrieli Foundation, and Rising Tide Foundation, Morris Kahn Institute for Human Immunology, and grants from the Benoziyo Endowment Fund for the Advancement of Science, Sir Charles Clore Research Prize, Comisaroff Family Trust, Irma and Jacques Ber-Lehmsdorf Foundation, Gerald O. Mann Charitable Foundation, and David M. Polen Charitable Trust.

Author contributions: N. Davidzohn designed and conducted the experiments, performed data analysis, and wrote the manuscript; A. Biram designed and performed experiments; L. Stoler-Barak generated transgenic mice; A. Grenov designed and performed the Kras experiments; B. Dassa performed and interpreted computational analyses; Z. Shulman designed experiments, supervised the study, and wrote the manuscript.

Disclosures: The authors declare no competing interests exist.

Submitted: 11 June 2019
Revised: 8 October 2019
Accepted: 18 November 2019

References

Adachi, T., J. Wienands, C. Wakabayashi, H. Yakura, M. Reth, and T. Tsubata. 2001. SHP-1 requires inhibitory co-receptors to down-modulate B cell antigen receptor-mediated phosphorylation of cellular substrates. *J. Biol. Chem.* 276:26648–26655. https://doi.org/10.1074/jbc.M100997200

Allen, C.D.C., T. Okada, H.L. Tang, and J.G. Cyster. 2007b. Imaging of germinal center selection events during affinity maturation. *Science.* 315: 528–531. https://doi.org/10.1126/science.1136736

Allen, D., T. Simon, F. Sablitzky, K. Rajewsky, and A. Cumano. 1988. Antibody engineering for the analysis of affinity maturation of an anti-hapten response. *EMBO J.* 7:1995–2001. https://doi.org/10.1002/j.1460-2075.1988.tb03038.x

Allen, C.D.C., K.M. Ansel, C. Low, R. Lesley, H. Tamamura, N. Fujii, and J.G. Cyster. 2004. Germinal center dark and light zone organization is mediated by CXCR4 and CXCR5. *Nat. Immunol.* 5:943–952. https://doi.org/10.1038/ni1100

Allen, C.D.C., T. Okada, and J.G. Cyster. 2007a. Germinal-center organization and cellular dynamics. *Immunity*. 27:190–202. https://doi.org/10.1016/j.immuni.2007.07.009

Anders, S., P.T. Pyl, and W. Huber. 2015. HTSeq--a Python framework to work with high-throughput sequencing data. *Bioinformatics*. 31:166–169. https://doi.org/10.1093/bioinformatics/btu638

Basso, K., and R. Dalla-Favera. 2015. Germinal centres and B cell lymphomagenesis. *Nat. Rev. Immunol.* 15:172–184. https://doi.org/10.1038/nri3814

Batista, F.D., and M.S. Neuberger. 2000. B cells extract and present immobilized antigen: implications for affinity discrimination. *EMBO J.* 19:513–520. https://doi.org/10.1093/emboj/19.4.513

Berek, C., A. Berger, and M. Apel. 1991. Maturation of the immune response in germinal centers. *Cell.* 67:1121–1129. https://doi.org/10.1016/0092-8674(91)90289-B

Biram, A., N. Davidzohn, and Z. Shulman. 2019. T cell interactions with B cells during germinal center formation, a three-step model. *Immunol. Rev.* 288:37–48. https://doi.org/10.1111/imr.12737

Calado, D.P., Y. Sasaki, S.A. Godinho, A. Pellerin, K. Köchert, B.P. Sleckman, I.M. de Alborán, M. Janz, S. Rodig, and K. Rajewsky. 2012. The cell-cycle regulator c-Myc is essential for the formation and maintenance of germinal centers. *Nat. Immunol.* 13:1092–1100. https://doi.org/10.1038/ni.2418

Chen, Y., Y. Zheng, X. You, M. Yu, G. Fu, X. Su, F. Zhou, W. Zhu, Z. Wu, J. Zhang, et al. 2016. Kras Is Critical for B Cell Lymphopoiesis. *J. Immunol.* 196:1678–1685. https://doi.org/10.4049/jimmunol.1502112

Cheng, A.M., B. Rowley, W. Pao, A. Hayday, J.B. Bolen, and T. Pawson. 1995. Syk tyrosine kinase required for mouse viability and B-cell development. *Nature.* 378:303–306. https://doi.org/10.1038/378303a0

Cumano, A., and K. Rajewsky. 1986. Clonal recruitment and somatic mutation in the generation of immunological memory to the hapten NP. *EMBO J.* 5:2459–2468. https://doi.org/10.1002/j.1460-2075.1986.tb04522.x

Dal Porto, J.M., S.B. Gauld, K.T. Merrell, D. Mills, A.E. Pugh-Bernard, and J. Cambier. 2004. B cell antigen receptor signaling 101. *Mol. Immunol.* 41:599–613. https://doi.org/10.1016/j.molimm.2004.04.008

De Silva, N.S., and U. Klein. 2015. Dynamics of B cells in germinal centres. *Nat. Rev. Immunol.* 15:137–148. https://doi.org/10.1038/nri3804

De Silva, N.S., M.M. Anderson, A. Carette, K. Silva, N. Heise, G. Bhagat, and U. Klein. 2016. Transcription factors of the alternative NF-κB pathway are required for germinal center B-cell development. *Proc. Natl. Acad. Sci. USA.* 113:9063–9068. https://doi.org/10.1073/pnas.1602728113

Deng, G.M., V.C. Kyttaris, and G.C. Tsokos. 2016. Targeting syk in autoimmune rheumatic diseases. *Front. Immunol.* 7:78. https://doi.org/10.3389/fimmu.2016.00078

Dobin, A., C.A. Davis, F. Schlesinger, J. Drenkow, C. Zaleski, S. Jha, P. Batut, M. Chaisson, and T.R. Gingeras. 2013. STAR: ultrafast universal RNA-seq aligner. *Bioinformatics*. 29:15–21. https://doi.org/10.1093/bioinformatics/bts635

Dominguez-Sola, D., G.D. Victora, C.Y. Ying, R.T. Phan, M. Saito, M.C. Nussenzweig, and R. Dalla-Favera. 2012. The proto-oncogene MYC is required for selection in the germinal center and cyclic reentry. *Nat. Immunol.* 13:1083–1091. https://doi.org/10.1038/ni.2428

Dominguez-Sola, D., J. Kung, A.B. Holmes, V.A. Wells, T. Mo, K. Basso, and R. Dalla-Favera. 2015. The FOXO1 Transcription Factor Instructs the Germinal Center Dark Zone Program. *Immunity*. 43:1064–1074. https://doi.org/10.1016/j.immuni.2015.10.015

Dustin, L.B., D.R. Plas, J. Wong, Y.T. Hu, C. Soto, A.C. Chan, and M.L. Thomas. 1999. Expression of dominant-negative src-homology domain 2-containing protein tyrosine phosphatase-1 results in increased Syk tyrosine kinase activity and B cell activation. *J. Immunol.* 162:2717–2724.

Edgar, R., M. Domrachev, and A.E. Lash. 2002. Gene Expression Omnibus: NCBI gene expression and hybridization array data repository. *Nucleic Acids Res.* 30:207–210. https://doi.org/10.1093/nar/30.1.207

Furukawa, K., A. Akasako-Furukawa, H. Shirai, H. Nakamura, and T. Azuma. 1999. Junctional amino acids determine the maturation pathway of an antibody. *Immunity*. 11:329–338. https://doi.org/10.1016/S1074-7613(00)80108-9

Gazumyan, A., A. Reichlin, and M.C. Nussenzweig. 2006. Ig β tyrosine residues contribute to the control of B cell receptor signaling by regulating receptor internalization. *J. Exp. Med.* 203:1785–1794. https://doi.org/10.1084/jem.20060221

Geahlen, R.L. 2009. Syk and pTyr'd: Signaling through the B cell antigen receptor. *Biochim. Biophys. Acta.* 1793:1115–1127. https://doi.org/10.1016/j.bbamcr.2009.03.004

Gitlin, A.D., Z. Shulman, and M.C. Nussenzweig. 2014. Clonal selection in the germinal centre by regulated proliferation and hypermutation. *Nature.* 509:637–640. https://doi.org/10.1038/nature13300

Gitlin, A.D., C.T. Mayer, T.Y. Oliveira, Z. Shulman, M.J.K. Jones, A. Koren, and M.C. Nussenzweig. 2015. HUMORAL IMMUNITY. T cell help controls the speed of the cell cycle in germinal center B cells. *Science.* 349:643–646. https://doi.org/10.1126/science.aac4919

Guo, F., Y. Luo, X. Jiang, X. Lu, D. Roberti, C. Lossos, K. Kunkalla, M. Magistri, L. Rui, R. Verdun, et al. 2019. Recent BCR stimulation induces a negative autoregulatory loop via FBXO10 mediated degradation of HGAL. *Leukemia.* https://doi.org/10.1038/s41375-019-0579-5

Heesters, B.A., R.C. Myers, and M.C. Carroll. 2014. Follicular dendritic cells: dynamic antigen libraries. *Nat. Rev. Immunol.* 14:495–504. https://doi.org/10.1038/nri3689

Herzog, S., M. Reth, and H. Jumaa. 2009. Regulation of B-cell proliferation and differentiation by pre-B-cell receptor signalling. *Nat. Rev. Immunol.* 9:195–205. https://doi.org/10.1038/nri2491

Ho, I.Y., J.J. Bunker, S.A. Erickson, K.E. Neu, M. Huang, M. Cortese, B. Pulendran, and P.C. Wilson. 2016. Refined protocol for generating monoclonal antibodies from single human and murine B cells. *J. Immunol. Methods.* 438:67–70. https://doi.org/10.1016/j.jim.2016.09.001

Ise, W., and T. Kurosaki. 2019. Plasma cell differentiation during the germinal center reaction. *Immunol. Rev.* 288:64–74. https://doi.org/10.1111/imr.12751

Ise, W., K. Fujii, K. Shiroguchi, A. Ito, K. Kometani, K. Takeda, E. Kawakami, K. Yamashita, K. Suzuki, T. Okada, and T. Kurosaki. 2018. T Follicular Helper Cell-Germinal Center B Cell Interaction Strength Regulates Entry into Plasma Cell or Recycling Germinal Center Cell Fate. *Immunity.* 48:702–715.e4. https://doi.org/10.1016/j.immuni.2018.03.027

Jackson, E.L., N. Willis, K. Mercer, R.T. Bronson, D. Crowley, R. Montoya, T. Jacks, and D.A. Tuveson. 2001. Analysis of lung tumor initiation and progression using conditional expression of oncogenic K-ras. *Genes Dev.* 15:3243–3248. https://doi.org/10.1101/gad.943001

Jaitin, D.A., E. Kenigsberg, H. Keren-Shaul, N. Elefant, F. Paul, I. Zaretsky, A. Mildner, N. Cohen, S. Jung, A. Tanay, and I. Amit. 2014. Massively parallel single-cell RNA-seq for marker-free decomposition of tissues into cell types. *Science.* 343:776–779. https://doi.org/10.1126/science.1247651

Khalil, A.M., J.C. Cambier, and M.J. Shlomchik. 2012. B cell receptor signal transduction in the GC is short-circuited by high phosphatase activity. *Science.* 336:1178–1181. https://doi.org/10.1126/science.1213368

Kitaura, Y., I.K. Jang, Y. Wang, Y.-C.C. Han, T. Inazu, E.J. Cadera, M. Schlissel, R.R. Hardy, and H. Gu. 2007. Control of the B cell-intrinsic tolerance programs by ubiquitin ligases Cbl and Cbl-b. *Immunity.* 26:567–578. https://doi.org/10.1016/j.immuni.2007.03.015

Kohen, R., J. Barlev, G. Hornung, G. Stelzer, E. Feldmesser, K. Kogan, M. Safran, and D. Leshkowitz. 2019. UTAP: User-friendly Transcriptome Analysis Pipeline. *BMC Bioinformatics.* 20:154. https://doi.org/10.1186/s12859-019-2728-2

Kräutler, N.J., D. Suan, D. Butt, K. Bourne, J.R. Hermes, T.D. Chan, C. Sundling, W. Kaplan, P. Schofield, J. Jackson, et al. 2017. Differentiation of germinal center B cells into plasma cells is initiated by high-affinity antigen and completed by Tfh cells. *J. Exp. Med.* 214:1259–1267. https://doi.org/10.1084/jem.20161533

Kulathu, Y., G. Grothe, and M. Reth. 2009. Autoinhibition and adapter function of Syk. *Immunol. Rev.* 232:286–299. https://doi.org/10.1111/j.1600-065X.2009.00837.x

Kurosaki, T., H. Shinohara, and Y. Baba. 2010. B cell signaling and fate decision. *Annu. Rev. Immunol.* 28:21–55. https://doi.org/10.1146/annurev.immunol.021908.132541

Kwak, K., N. Quizon, H. Sohn, A. Saniee, J. Manzella-Lapeira, P. Holla, J. Brzostowski, J. Lu, H. Xie, C. Xu, et al. 2018. Intrinsic properties of human germinal center B cells set antigen affinity thresholds. *Sci. Immunol.* 3:eaau6598. https://doi.org/10.1126/sciimmunol.aau6598

Laidlaw, B.J., T.H. Schmidt, J.A. Green, C.D.C. Allen, T. Okada, and J.G. Cyster. 2017. The Eph-related tyrosine kinase ligand Ephrin-B1 marks germinal center and memory precursor B cells. *J. Exp. Med.* 214:639–649. https://doi.org/10.1084/jem.20161461

Li, X., A. Gadzinsky, L. Gong, H. Tong, V. Calderon, Y. Li, D. Kitamura, U. Klein, W.Y. Langdon, F. Hou, et al. 2018. Cbl Ubiquitin Ligases Control B Cell Exit from the Germinal-Center Reaction. *Immunity*. 48: 530–541.e6. https://doi.org/10.1016/j.immuni.2018.03.006

Love, M.I., W. Huber, and S. Anders. 2014. Moderated estimation of fold change and dispersion for RNA-seq data with DESeq2. *Genome Biol*. 15: 550. https://doi.org/10.1186/s13059-014-0550-8

Luo, W., F. Weisel, and M.J. Shlomchik. 2018. B Cell Receptor and CD40 Signaling Are Rewired for Synergistic Induction of the c-Myc Transcription Factor in Germinal Center B Cells. *Immunity*. 48:313–326.e5. https://doi.org/10.1016/j.immuni.2018.01.008

Luo, W., W. Hawse, L. Conter, N. Trivedi, F. Weisel, D. Wikenheiser, R.T. Cattley, and M.J. Shlomchik. 2019. The AKT kinase signaling network is rewired by PTEN to control proximal BCR signaling in germinal center B cells. *Nat. Immunol.* 20:736–746. https://doi.org/10.1038/s41590-019-0376-3

Lupher, M.L. Jr., N. Rao, N.L. Lill, C.E. Andoniou, S. Miyake, E.A. Clark, B. Druker, and H. Band. 1998. Cbl-mediated negative regulation of the Syk tyrosine kinase. A critical role for Cbl phosphotyrosine-binding domain binding to Syk phosphotyrosine 323. *J. Biol. Chem.* 273:35273–35281. https://doi.org/10.1074/jbc.273.52.35273

MacLennan, I.C. 1994. Germinal centers. *Annu. Rev. Immunol.* 12:117–139. https://doi.org/10.1146/annurev.iy.12.040194.001001

Minnich, M., H. Tagoh, P. Bönelt, E. Axelsson, M. Fischer, B. Cebolla, A. Tarakhovsky, S.L. Nutt, M. Jaritz, and M. Busslinger. 2016. Multifunctional role of the transcription factor Blimp-1 in coordinating plasma cell differentiation. *Nat. Immunol.* 17:331–343. https://doi.org/10.1038/ni.3349

Mócsai, A., J. Ruland, and V.L.J.J. Tybulewicz. 2010. The SYK tyrosine kinase: a crucial player in diverse biological functions. *Nat. Rev. Immunol.* 10: 387–402. https://doi.org/10.1038/nri2765

Mootha, V.K., C.M. Lindgren, K.-F. Eriksson, A. Subramanian, S. Sihag, J. Lehar, P. Puigserver, E. Carlsson, M. Ridderstråle, E. Laurila, et al. 2003. PGC-1α-responsive genes involved in oxidative phosphorylation are coordinately downregulated in human diabetes. *Nat. Genet.* 34:267–273. https://doi.org/10.1038/ng1180

Mueller, J., M. Matloubian, and J. Zikherman. 2015. Cutting edge: An in vivo reporter reveals active B cell receptor signaling in the germinal center. *J. Immunol.* 194:2993–2997. https://doi.org/10.4049/jimmunol.1403086

Niu, H., B.H. Ye, and R. Dalla-Favera. 1998. Antigen receptor signaling induces MAP kinase-mediated phosphorylation and degradation of the BCL-6 transcription factor. *Genes Dev.* 12:1953–1961. https://doi.org/10.1101/gad.12.13.1953

Nutt, S.L., P.D. Hodgkin, D.M. Tarlinton, and L.M. Corcoran. 2015. The generation of antibody-secreting plasma cells. *Nat. Rev. Immunol.* 15: 160–171. https://doi.org/10.1038/nri3795

Ochiai, K., M. Maienschein-Cline, G. Simonetti, J. Chen, R. Rosenthal, R. Brink, A.S. Chong, U. Klein, A.R. Dinner, H. Singh, and R. Sciammas. 2013. Transcriptional regulation of germinal center B and plasma cell fates by dynamical control of IRF4. *Immunity*. 38:918–929. https://doi.org/10.1016/j.immuni.2013.04.009

Oh-hora, M., S. Johmura, A. Hashimoto, M. Hikida, and T. Kurosaki. 2003. Requirement for Ras guanine nucleotide releasing protein 3 in coupling phospholipase C-γ2 to Ras in B cell receptor signaling. *J. Exp. Med.* 198: 1841–1851. https://doi.org/10.1084/jem.20031547

Pao, L.I., J.C. Cambier, W. Song, and S.K. Pierce. 1997. Syk, but not Lyn, recruitment to B cell antigen receptor and activation following stimulation of CD45- B cells. *J. Immunol.* 158:2663–2669. https://doi.org/10.4049/jimmunol.166.6.3693

Perova, T., I. Grandal, L.M.J. Nutter, E. Papp, I.R. Matei, J. Beyene, P.E. Kowalski, J.K. Hitzler, M.D. Minden, C.J. Guidos, and J.S. Danska. 2014. Therapeutic potential of spleen tyrosine kinase inhibition for treating high-risk precursor B cell acute lymphoblastic leukemia. *Sci. Transl. Med.* 6:236ra62. https://doi.org/10.1126/scitranslmed.3008661

Phan, T.G., M. Amesbury, S. Gardam, J. Crosbie, J. Hasbold, P.D. Hodgkin, A. Basten, and R. Brink. 2003. B cell receptor-independent stimuli trigger immunoglobulin (Ig) class switch recombination and production of IgG autoantibodies by anergic self-reactive B cells. *J. Exp. Med.* 197:845–860. https://doi.org/10.1084/jem.20022144

Rao, N., I. Dodge, and H. Band. 2002. The Cbl family of ubiquitin ligases: critical negative regulators of tyrosine kinase signaling in the immune system. *J. Leukoc. Biol.* 71:753–763. https://doi.org/10.1189/JLB.71.5.753

Rawlings, D.J., G. Metzler, M. Wray-Dutra, and S.W. Jackson. 2017. Altered B cell signalling in autoimmunity. *Nat. Rev. Immunol.* 17:421–436. https://doi.org/10.1038/nri.2017.24

Reth, M., and J. Wienands. 1997. Initiation and processing of signals from the B cell antigen receptor. *Annu. Rev. Immunol.* 15:453–479. https://doi.org/10.1146/annurev.immunol.15.1.453

Sander, S., D.P. Calado, L. Srinivasan, K. Köchert, B. Zhang, M. Rosolowski, S.J. Rodig, K. Holzmann, S. Stilgenbauer, R. Siebert, et al. 2012. Synergy between PI3K signaling and MYC in Burkitt lymphomagenesis. *Cancer Cell.* 22:167–179. https://doi.org/10.1016/j.ccr.2012.06.012

Sander, S., V.T. Chu, T. Yasuda, A. Franklin, R. Graf, D.P. Calado, S. Li, K. Imami, M. Selbach, M. Di Virgilio, et al. 2015. PI3 Kinase and FOXO1 Transcription Factor Activity Differentially Control B Cells in the Germinal Center Light and Dark Zones. *Immunity*. 43:1075–1086. https://doi.org/10.1016/j.immuni.2015.10.021

Satpathy, S., S.A. Wagner, P. Beli, R. Gupta, T.A. Kristiansen, D. Malinova, C. Francavilla, P. Tolar, G.A. Bishop, B.S. Hostager, and C. Choudhary. 2015. Systems-wide analysis of BCR signalosomes and downstream phosphorylation and ubiquitylation. *Mol. Syst. Biol.* 11:810. https://doi.org/10.15252/msb.20145880

Schwickert, T.A., R.L. Lindquist, G. Shakhar, G. Livshits, D. Skokos, M.H. Kosco-Vilbois, M.L. Dustin, and M.C. Nussenzweig. 2007. In vivo imaging of germinal centres reveals a dynamic open structure. *Nature*. 446:83–87. https://doi.org/10.1038/nature05573

Sciammas, R., A.L. Shaffer, J.H. Schatz, H. Zhao, L.M. Staudt, and H. Singh. 2006. Graded expression of interferon regulatory factor-4 coordinates isotype switching with plasma cell differentiation. *Immunity*. 25: 225–236. https://doi.org/10.1016/j.immuni.2006.07.009

Setz, C.S., E. Hug, A. Khadour, H. Abdelrasoul, M. Bilal, E. Hobeika, and H. Jumaa. 2018. PI3K-Mediated Blimp-1 Activation Controls B Cell Selection and Homeostasis. *Cell Reports*. 24:391–405. https://doi.org/10.1016/j.celrep.2018.06.035

Sharma, S., G. Orlowski, and W. Song. 2009. Btk regulates B cell receptor-mediated antigen processing and presentation by controlling actin cytoskeleton dynamics in B cells. *J. Immunol.* 182:329–339. https://doi.org/10.4049/jimmunol.182.1.329

Shi, W., Y. Liao, S.N. Willis, N. Taubenheim, M. Inouye, D.M. Tarlinton, G.K. Smyth, P.D. Hodgkin, S.L. Nutt, and L.M. Corcoran. 2015. Transcriptional profiling of mouse B cell terminal differentiation defines a signature for antibody-secreting plasma cells. *Nat. Immunol.* 16:663–673. https://doi.org/10.1038/ni.3154

Shih, T.-A.Y., M. Roederer, and M.C. Nussenzweig. 2002a. Role of antigen receptor affinity in T cell-independent antibody responses in vivo. *Nat. Immunol.* 3:399–406. https://doi.org/10.1038/ni776

Shih, T.A.Y., E. Meffre, M. Roederer, and M.C. Nussenzweig. 2002b. Role of BCR affinity in T cell dependent antibody responses in vivo. *Nat. Immunol.* 3:570–575. https://doi.org/10.1038/ni803

Shlomchik, M.J., W. Luo, and F. Weisel. 2019. Linking signaling and selection in the germinal center. *Immunol. Rev.* 288:49–63. https://doi.org/10.1111/imr.12744

Sohn, H.W., H. Gu, and S.K. Pierce. 2003. Cbl-b negatively regulates B cell antigen receptor signaling in mature B cells through ubiquitination of the tyrosine kinase Syk. *J. Exp. Med.* 197:1511–1524. https://doi.org/10.1084/jem.20021686

Song, J., N. Uyttersprot, S. Classen, and A. Waisman. 2016. The IgG1 B-cell receptor provides survival and proliferative signals analogue to the Igα but not the Igβ co-receptor. *Eur. J. Immunol.* 46:1878–1886. https://doi.org/10.1002/eji.201646396

Srinivasan, L., Y. Sasaki, D.P. Calado, B. Zhang, J.H. Paik, R.A. DePinho, J.L. Kutok, J.F. Kearney, K.L. Otipoby, and K. Rajewsky. 2009. PI3 kinase signals BCR-dependent mature B cell survival. *Cell.* 139:573–586. https://doi.org/10.1016/j.cell.2009.08.041

Suan, D., C. Sundling, and R. Brink. 2017. Plasma cell and memory B cell differentiation from the germinal center. *Curr. Opin. Immunol.* 45: 97–102. https://doi.org/10.1016/j.coi.2017.03.006

Subramanian, A., P. Tamayo, V.K. Mootha, S. Mukherjee, B.L. Ebert, M.A. Gillette, A. Paulovich, S.L. Pomeroy, T.R. Golub, E.S. Lander, and J.P. Mesirov. 2005. Gene set enrichment analysis: a knowledge-based approach for interpreting genome-wide expression profiles. *Proc. Natl. Acad. Sci. USA*. 102:15545–15550. https://doi.org/10.1073/pnas.0506580102

Suzuki, K., I. Grigorova, T.G. Phan, L.M. Kelly, and J.G. Cyster. 2009. Visualizing B cell capture of cognate antigen from follicular dendritic cells. *J. Exp. Med.* 206:1485–1493. https://doi.org/10.1084/jem.20090209

Turner, M., P.J. Mee, P.S. Costello, O. Williams, A.A. Price, L.P. Duddy, M.T. Furlong, R.L. Geahlen, and V.L.J. Tybulewicz. 1995. Perinatal lethality and blocked B-cell development in mice lacking the tyrosine kinase Syk. *Nature*. 378:298–302. https://doi.org/10.1038/378298a0

Victora, G.D., and M.C. Nussenzweig. 2012. Germinal centers. *Annu. Rev. Immunol.* 30:429–457. https://doi.org/10.1146/annurev-immunol-020711-075032

Victora, G.D., T.A. Schwickert, D.R. Fooksman, A.O. Kamphorst, M. Meyer-Hermann, M.L. Dustin, and M.C. Nussenzweig. 2010. Germinal center dynamics revealed by multiphoton microscopy with a photoactivatable fluorescent reporter. *Cell.* 143:592–605. https://doi.org/10.1016/j.cell.2010.10.032

von Boehmer, L., C. Liu, S. Ackerman, A.D. Gitlin, Q. Wang, A. Gazumyan, and M.C. Nussenzweig. 2016. Sequencing and cloning of antigen-specific antibodies from mouse memory B cells. *Nat. Protoc.* 11:1908–1923. https://doi.org/10.1038/nprot.2016.102

Wang, H., H. Yang, C.S. Shivalila, M.M. Dawlaty, A.W. Cheng, F. Zhang, and R. Jaenisch. 2013. One-step generation of mice carrying mutations in multiple genes by CRISPR/Cas-mediated genome engineering. *Cell.* 153:910–918. https://doi.org/10.1016/j.cell.2013.04.025

Weisel, F., and M. Shlomchik. 2017. Memory B Cells of Mice and Humans. *Annu. Rev. Immunol.* 35:255–284. https://doi.org/10.1146/annurev-immunol-041015-055531

Weisel, F.J., G.V. Zuccarino-Catania, M. Chikina, and M.J. Shlomchik. 2016. A Temporal Switch in the Germinal Center Determines Differential Output of Memory B and Plasma Cells. *Immunity.* 44:116–130. https://doi.org/10.1016/j.immuni.2015.12.004

Yankee, T.M., L.M. Keshvara, S. Sawasdikosol, M.L. Harrison, and R.L. Geahlen. 1999. Inhibition of signaling through the B cell antigen receptor by the protooncogene product, c-Cbl, requires Syk tyrosine 317 and the c-Cbl phosphotyrosine-binding domain. *J. Immunol.* 163:5827–5835.

Yasuda, T., K. Kometani, N. Takahashi, Y. Imai, Y. Aiba, and T. Kurosaki. 2011. ERKs induce expression of the transcriptional repressor Blimp-1 and subsequent plasma cell differentiation. *Sci. Signal.* 4:ra25. https://doi.org/10.1126/scisignal.2001592

Yasuda, T., F. Hayakawa, S. Kurahashi, K. Sugimoto, Y. Minami, A. Tomita, and T. Naoe. 2012. B cell receptor-ERK1/2 signal cancels PAX5-dependent repression of BLIMP1 through PAX5 phosphorylation: a mechanism of antigen-triggering plasma cell differentiation. *J. Immunol.* 188:6127–6134. https://doi.org/10.4049/jimmunol.1103039

Yusuf, I., X. Zhu, M.G. Kharas, J. Chen, and D.A. Fruman. 2004. Optimal B-cell proliferation requires phosphoinositide 3-kinase-dependent inactivation of FOXO transcription factors. *Blood.* 104:784–787. https://doi.org/10.1182/blood-2003-09-3071

Supplemental material

Davidzohn et al., https://doi.org/10.1084/jem.20191043

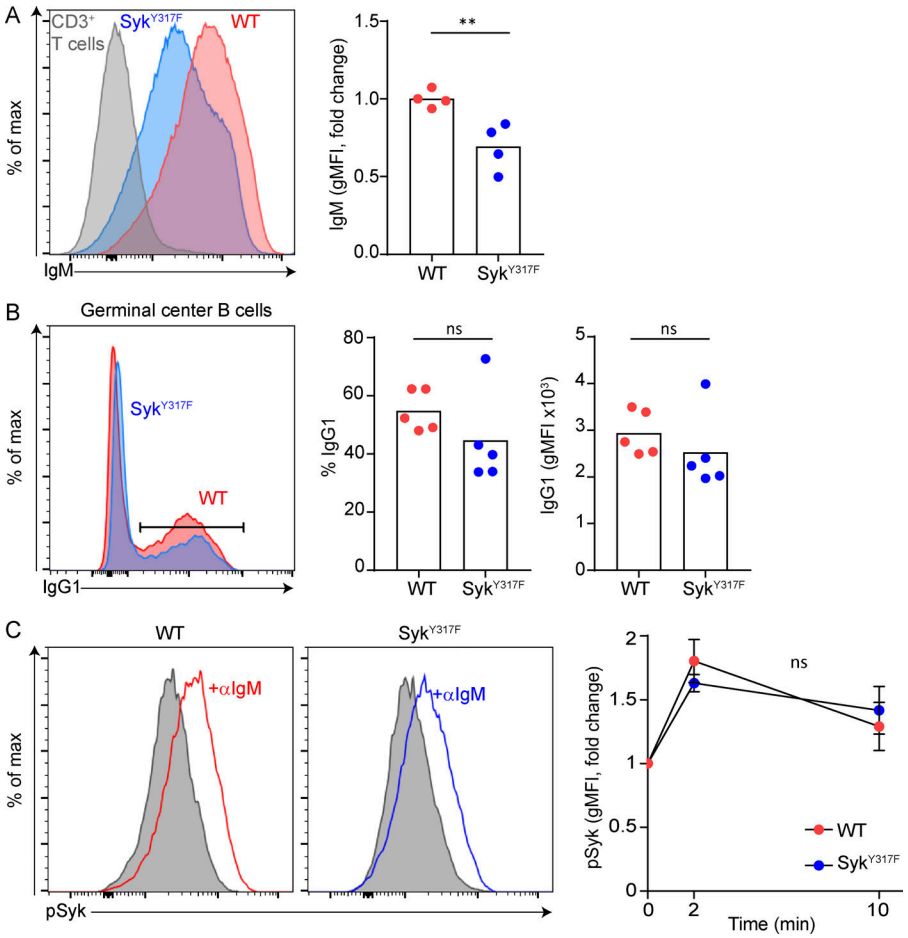

Figure S1. **IgM and IgG1 expression and Syk phosphorylation at position Y348 in WT and Syk^{Y317F} mice. (A and B)** Flow cytometry analysis and quantification of IgM expression on WT and Syk^{Y317F} follicular B cells (A) and IgG1 expression on WT and Syk^{Y317F} GC B cells (B220^{+} FAS^{+} CD38^{low}; B; *n* = 4 in A and *n* = 5 in B, two independent experiments, two-tailed Student's *t* test). Each dot in the graphs represents a single mouse; bars represent the mean. **(C)** Flow cytometry histograms and quantification of pSyk in WT and Syk^{Y317F} B cells that were left unstimulated or stimulated with anti-IgM at different time points. The gMFI of pSyk (Tyr 348) after 2 and 10 min of stimulation was normalized to the gMFI at time 0. Each graph represents the mean of ± SEM (*n* = 3, three independent experiments, two-tailed Student's *t* test). **, P ≤ 0.01; ns, not significant.

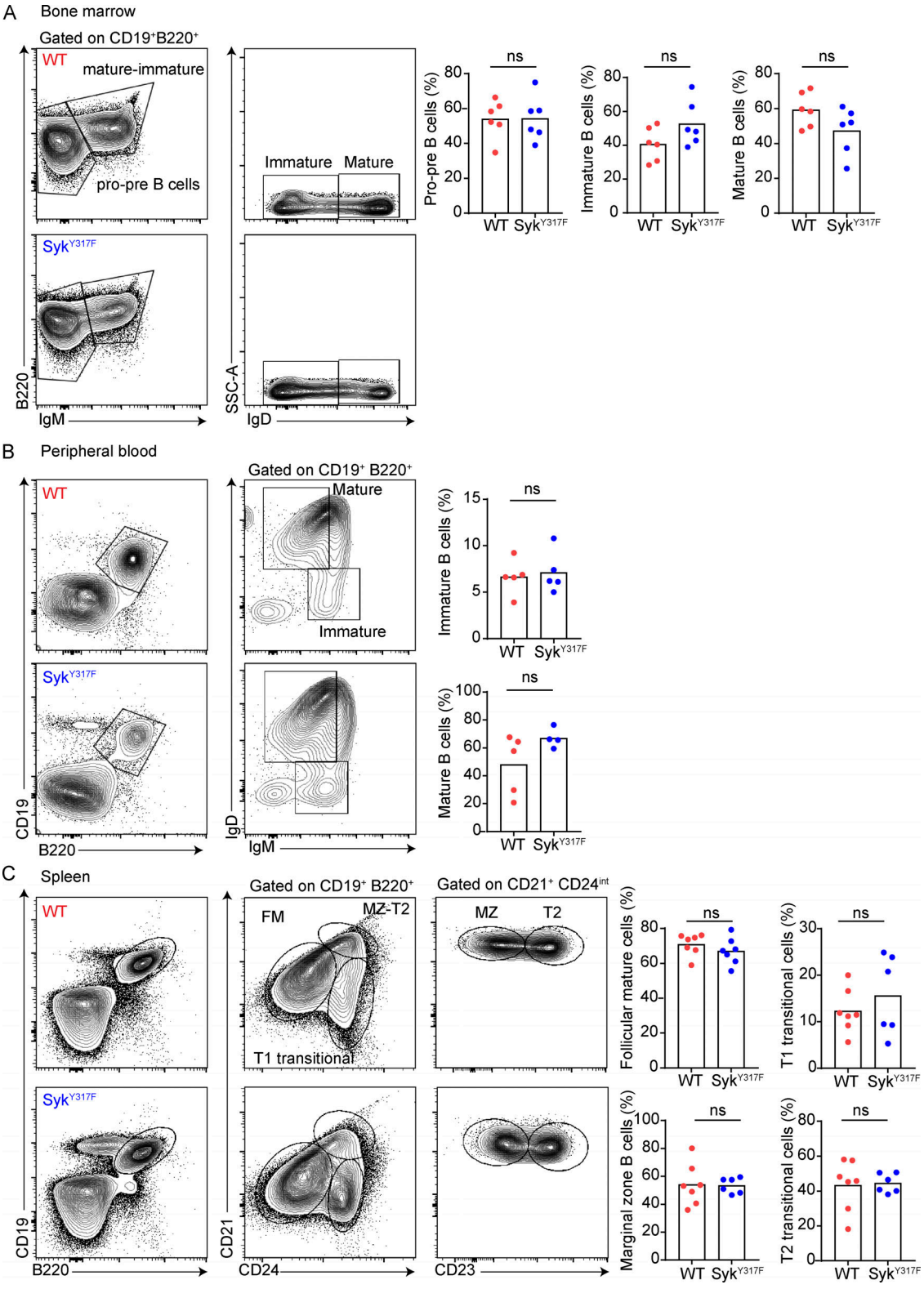

Figure S2. **Syk^{Y317F} mice exhibit normal B cell development. (A–C)** Representative flow-cytometric analysis and quantification of Syk^{Y317F} and WT B cells in different developmental stages in the BM (A), peripheral blood (B), and spleen (C). Each dot represents a single mouse; bars represent the mean (n = 4–7, two independent experiments, two-tailed Student's t test). ns, not significant.

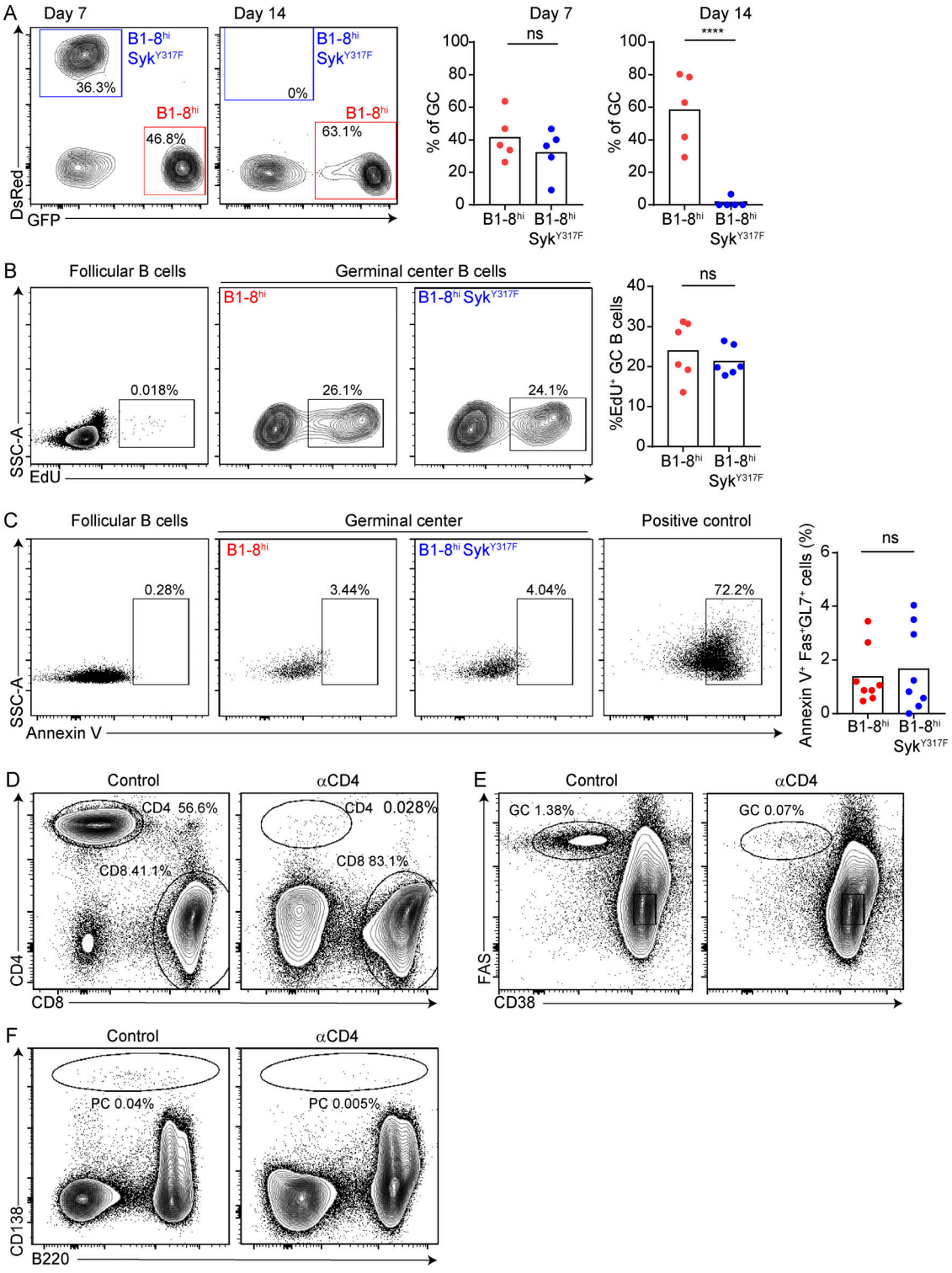

Figure S3. **Syk degradation is required for B cell persistence in GCs independently of their relative BCR affinity in a T cell–dependent manner. (A)** Analysis of transferred B1-8^{hi} and B1-8^{hi} Syk^{Y317F} B cells in GCs (B220^{+} FAS^{+}CD38^{low}) in MD4 recipient mice 7 and 14 d after immunization with NP-OVA. Each dot in the graphs represents a single mouse; bars represent the mean (n = 5, two independent experiments, two-tailed Student's t test). **(B and C)** Representative flow-cytometric analysis and quantification of EdU^{+} (B) and Annexin V^{+} (C) in B1-8^{hi} and B1-8^{hi} Syk^{Y317F} B cells that were cotransferred into WT hosts. Mice were immunized with NP-OVA, and GCs were analyzed 7 d later. Each dot in the graphs represents a single mouse; bars represent the mean (n = 6–8, two independent experiments, two-tailed Student's t test). **(D–F)** Gating strategy for CD4^{+} T cells (D), GC B cells (E), and PCs (F) following CD4-depleting antibody or PBS injection into NP-KLH–immunized chimeric mice (~50% GFP^{+}, ~50% Syk^{Y317F}). Quantification of the data are shown in Fig. 4 C. ****, P < 0.0001; ns, not significant.

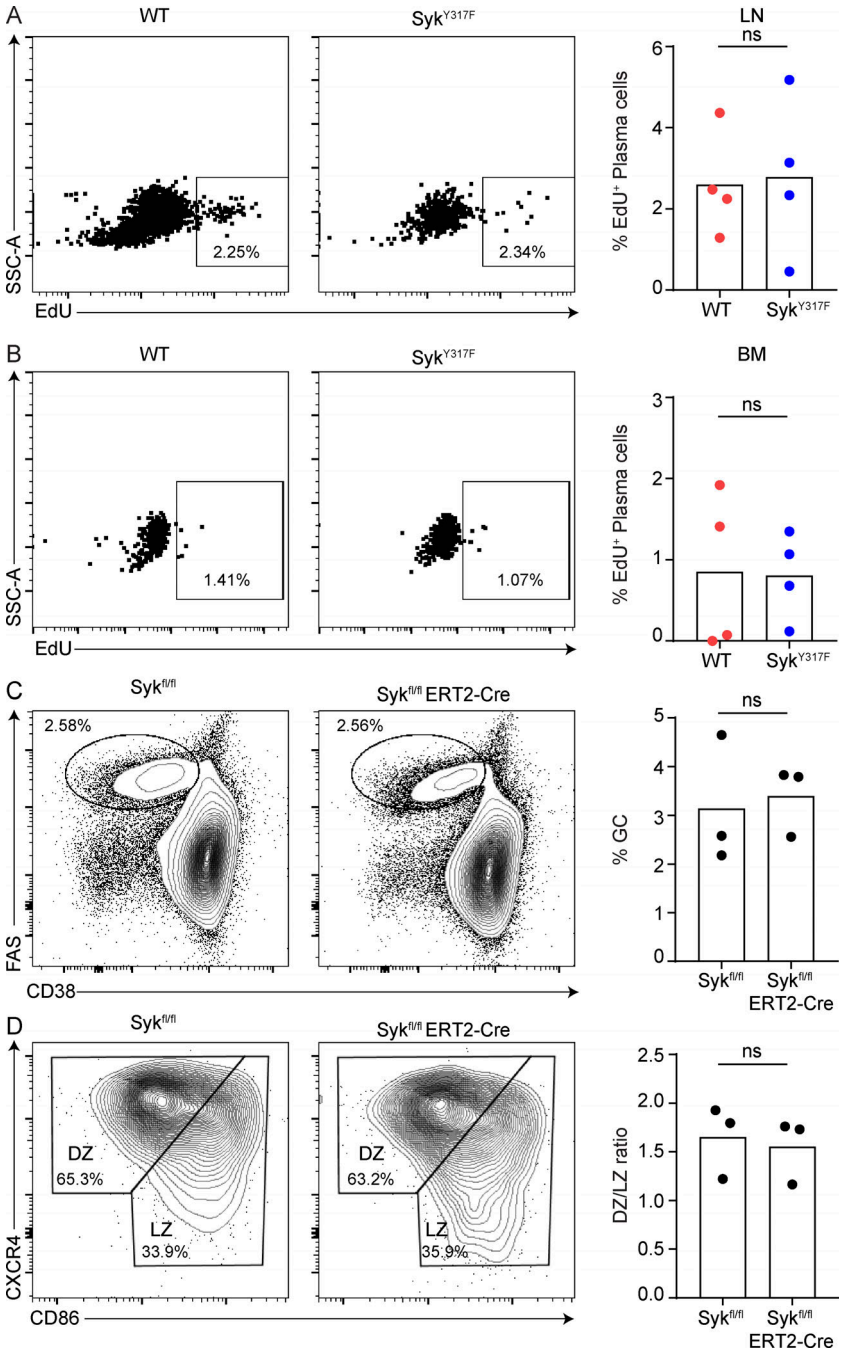

Figure S4. **Short-term EdU incorporation in PCs and ERT2-Cre expression effect on the GC reaction. (A and B)** Representative flow-cytometric plots and quantification of EdU+ PCs (CD138+) in popliteal lymph nodes (A) of NP-KLH immunized mice (day 14) and in the BM (B) 2.5 h after injection of EdU into immunized mice (n = 4, two independent experiments, two-tailed Student's t test). **(C and D)** Representative flow-cytometric plots and quantification of GC size (C), DZ, and LZ (D) GC B cell distribution in Syk$^{fl/fl}$ and Syk$^{fl/fl}$ ERT2-Cre mice 7 d after immunization without tamoxifen treatment. Each dot in the graphs represents a single mouse; bars represent the mean (n = 3, one experiment, two-tailed Student's t test). ns, not significant; SSC-A, side scatter–area.

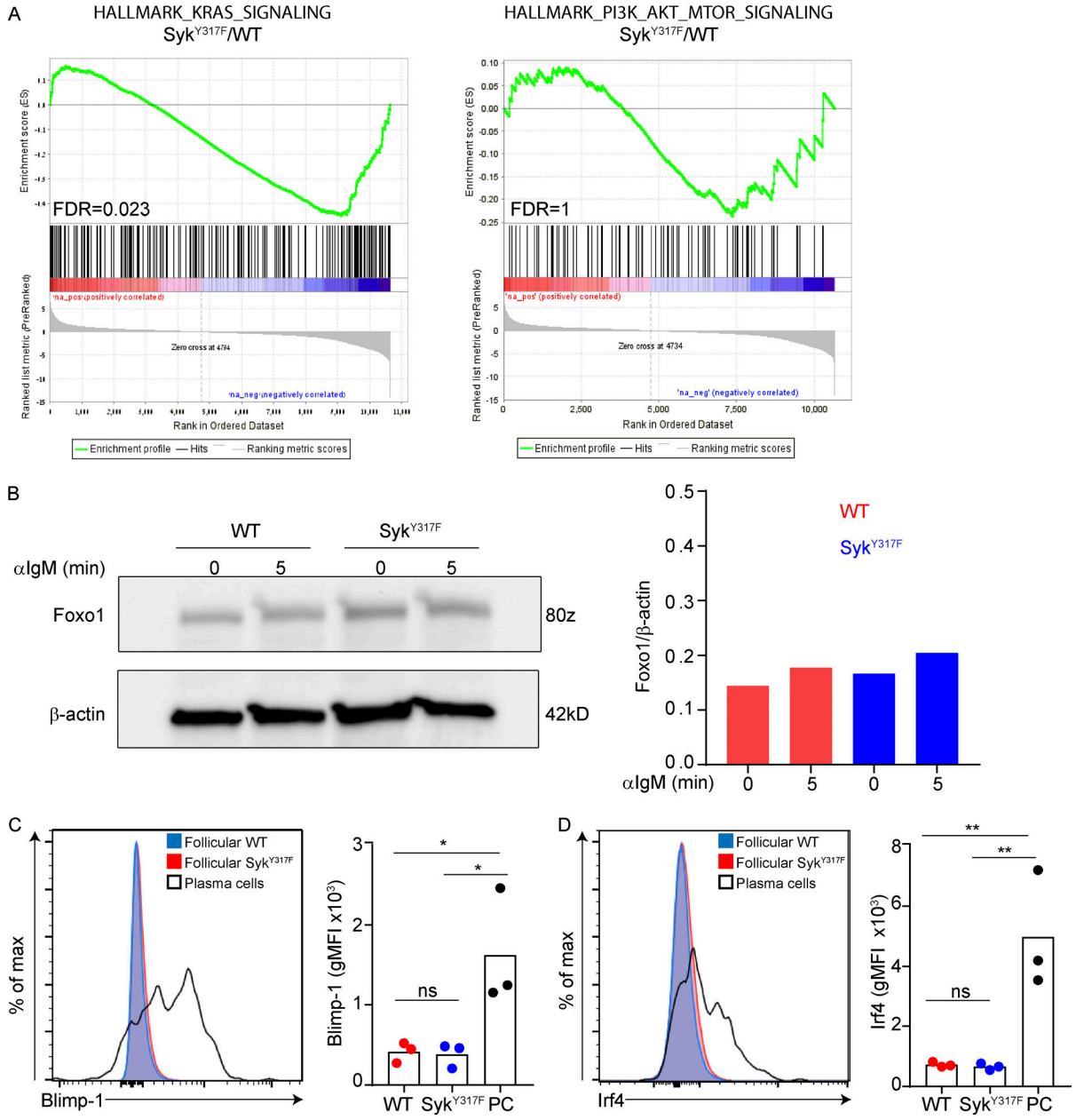

Figure S5. **Changes in gene expression that are related to the Kras and PI3K pathways in WT and Syk^{Y317F} mice. (A)** GSEA plot showing enrichment of the Kras and PI3K/Akt/MTOR signaling pathways in LZ GC B cells. False discovery rate q value = 0.023 and false discovery rate q value= 1, respectively. Analysis is based on the gene expression data shown in Fig. 6. **(B)** Foxo1 protein levels were determined by Western blot analysis of B cells derived from WT and Syk^{Y317F} mice that were stimulated with anti-IgM for the indicated time. Signals were normalized to β-actin (n = 1, one experiment). **(C and D)** Representative histograms and quantification of Blimp-1 (C) and Irf4 (D) expression in follicular B cells (B220$^+$FAS$^+$CD38^{hi}) and PCs (CD138$^+$) of WT and Syk^{Y317F} mice. Each dot in the graphs represents a single mouse; bars represent the mean (n = 3, one experiment, two-tailed Student's t test). ns, not significant; *, P = 0.05; **, P ≤ 0.01.

Table S1. **List of antibodies used for flow cytometry**

Antigen	Fluorophore	Clone	Manufacturer	Concentration, µg/ml
B220	V500	RA3-6B2	BD	1
B220	APC-Alexa Fluor 780/e450	RA3-6B2	eBioscience	1
CD138	BV605	281-2	Biolegend	0.5
CD38	FITC	90	Biolegend	1
CD38	Alexa Fluor 700	90	eBioscience	1
F4/80	APC-Alexa Fluor 780	BM8	eBioscience	1
FAS	PE-Cy7	Jo2	BD	0.33
GL-7	Alexa Fluor 647/PerCP-Cy5.5	GL7	Biolegend	2.5
Gr-1	APC-Alexa Fluor 780	RB6-8C5	eBioscience	1
Igλ	PE	RML-42	Biolegend	1
Streptavidin	Alexa Fluor 647		Biolegend	1
IgM	Biotin	RMM-1	Biolegend	1
IgM	PerCP-CeFluor710	II/41	eBioscience	1
IgG1	BV421/FITC	RMG1-1	Biolegend	1
IgD	Alexa Fluor 647	11-26c.2a	Biolegend	1
CD4	Alexa Fluor 488/Alexa Fluor 780	GK1.5	Biolegend	1
CD8	Pacific Blue	53-6.7	Biolegend	1
CD8	Alexa Fluor 780	53-6.7	eBioscience	1
CD19	Pacific Blue	6D5	Biolegend	1
CD19	FITC	MB19-1	Biolegend	1
CD3	PE	145-2C11	Biolegend	1
CD21	APC-Cy7	7E9	Biolegend	1
CD24	PeCy7	M1/69	Biolegend	1
CD23	FITC	B3B4	Biolegend	1
CXCR4	BV421	L276F12	Biolegend	1
CD86	PE/FITC	GL-1	Biolegend	0.08
pERK	Alexa Fluor 488	4B11B69	Biolegend	2.5
CD45.1	BV421	A20	Biolegend	1
CD45.1	Alexa Fluor 780	A20	eBioscience	1
CD45.2	PE	104	Biolegend	1
Blimp-1	Alexa Fluor 647	5E7	Biolegend	1
Irf4	Alexa Fluor 488/PerCP-Cy5.5	IRF4.3E4	Biolegend	1
p-S6 (Ser235/236)	Alexa Fluor 647	D57.2.2E	Cell Signaling Technology	1
pSyk ab	PE	moch1ct	eBioscience	1

Table S2. **List of primers used for Igγ1 sequencing**

Primers	**Primer sequence 5′-3′**
Variable region primers	
HP1F-mLEADER-1	GTAACACTTTTAAATGGTATCCAGTGT
HP1F-mLEADER-2	GTCCTAATTTTAAAAGGTGTCCAGTGT
HP1F-mLEADER-3	AGCAACAGCTACAGGTGTCCACTCC
HP1F-mLEADER-4	TCTTCTTCCTGTCAGTAACTRCAGG
HP1F-mLEADER-5	TTGCTATTCCTGATGGCAGCTGCCCAA
HP1F-mLEADER-6	GTGACATTCCCAAGCTGTGTCCTRTCC
HP1F-mLEADER-7	TGTACCTGTTGACAGTCGTTCCTGG
HP1F-mLEADER-8	GTTTTTTATCAAGGTGTGCATTGT
HP1F-mLEADER-9	CTATTCCTGATGGCAGCTGCCCAAAG
VH186.2 variable region primer	CTAGTAGCAACTGCAACCGGTGTACATTCTCAGGTGCAGCTGCAGGAGTC
Constant region primers	
Cγ1-outer	GGAAGGTGTGCACACCGCTGGAC
Cγ1-inner	GCTCAGGGAAATAGCCCTTGAC